CO4-1 Crystal structure analysis of aragonite by neutron diffraction

K. Iwase[1] and K. Mori[2]

[1]*Department of Materials Science and Engineering, Ibaraki University*

[2]*KURNS, Kyoto University*

INTRODUCTION: Creatures form biominerals such as shell, bone, pearl, eggshell, exoskeleton, etc. The process of forming those minerals, which is called biomineralization, takes place usually at ambient temperature and pressure. Biominerals are nanocomposite materials made of inorganic and organic substances [1] and renowned for their mechanical property [2].

The crystal structures of calcium carbonate were reported by Terada [3]. Calcium carbonate have three polymorphs: aragonite, calcite and vaterite phases. Calcite is stable phase among three polymocphs, while aragonite and vaterite are unstable phases in the temperature range 273 K to 1243 K. The aragonite phase is orthorhombic with the space group of *Pnma*, while the calcite phase is trigonal with the spae group of *R*-3*c*. The vaterite phase has the $P6_3/mmc$ spece group. Among shells, Tapes philippinarum, Meretrix lusoria, corbicula, etc, are composed of the aragonite phases, while oyster and scallop shell are of the calcite one. The vaterite phase is seldom obtained in the usual biological systems.

Taylor and Layman reported the mechanical propertys and structures of bivalve shell [2]. The mechanical properties were investigated by bending, impact and microhardness tests. Seven to ten specimens, Pinctada martensi, Mercenaria mercenaria, Glycymeris glycymeris, Pecten maximus, etc, were used for the tests. Pinctada martensi with nacre structure indicated highest stress at fracture by bending and impact tests. The microhrardness of various shell structures, aragonite prisms, composite prisms, sheet nacre and crossed-lamellar, etc, were measured. The microhardness of composite prisms was harder than other structures. The shell of Strombus gigas is formed with 95 % (by volume) inorganic phase and 5 % organic phase. The nacre of Strombus gigas is 3000 times as tough as its pure constituent mineral [4]. The texture of nacre of Strombus gigas is called crossed lamellar microarchitecture, which affords uncracked structural feature of surface [6]. Strombus gigas contains structure at five distinct length scales and the texture size is controlled from 5 μm to 2 mm.

In this study, aragonite was synthesized for NPD measurement. Structural parameters of synthesized aragonite were refined by Rietveld method.

EXPERIMENTS: NPD data were collected by using the step-scan mode of a diffractometer (B-3) with 1.0294 Å wavelength. The powdered sample was sieved to a particle size of < 20 μm for the NPD measurements.

Synthesized aragonite was prepared by the following procedure. An 1.0-L Erlenmeyer flask was used as the reactor, and 1.6 g $NaHCO_3$ was added slowly to an aqueous solution (600 mL) containing 0.8 g $CaCl_2$ at 353 K. During the reaction, the sample was stirred at 1030 rpm. The aragonite phase could be synthesized in the laboratory under stirring at high temperature, when there is no Mg^{2+} in the solution.

RESULTS: Rietveld refinement pattern of synthesized aragonite is shown in Fig. 1. The structural model based on space group $P6_3/mmc$ was developed. The goodness of fit *S* was 1.8. The refined lattice parameters *a*, *b* and *c* were 0.5739(3), 0.4962(2) and 0.7968(4) nm, respectively, which agreed with the values reported by Terada [3]. The refined lattice parameters and atomic position of synthesized are obtained using B-3. In the next stage, biogenic aragonite will be measured by B-3.

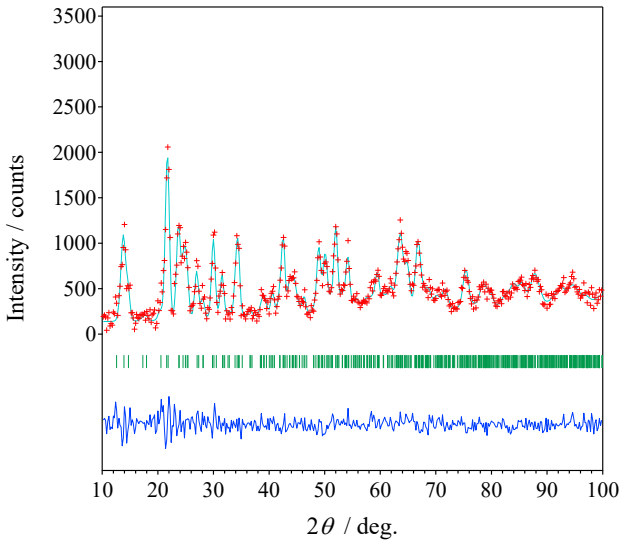

Fig. 1 NPD profile of synthesized aragonite

REFERENCES:

[1] Y. Dauphin, Structures, organo-mineral compositions and diagenetic changes in biominerals, Curr. Opin. Colloid. Interface. Sci. 7 (2002) 133-138.

[2] Y. Dauphin, J.P. Cuif, J. Doucet, M. Salome, J. Susini, C.T.Willams, In situ chemical speciation of sulfur in calcitic biominerals and the simple prism concept, J. Struct. Biol. 142 (2003) 272-280.

[3] J. Terada, Crystal structure of the Ba, Sr, and Ca triple carbonate, J. Phys. Soc. Jpn. 8(2) (1953) 158-164.

[4] A.P. Jackson, J.F.V. Vincent, R.M. TURNER, The mechanical design of nacre, Proc. R. Soc. Lond. B 234 (1988) 415–440.

[5] S. Kamat, X. Su, R. Ballarini, A. H. Heuer, Structural basis for the fracture toughness of the shell of the conch Strombus gigas, Nature 405 (2000) 1036-1040.

CO4-2

Radiochemical Research for the Advancement of $^{99}Mo/^{99m}Tc$ Generator by (n, γ) Method

Y. Fujita, M. Seki, Y. Namekawa, K. Nishikata, A. Kimura, A. Shibata, N. Sayato, K. Tsuchiya, T. Sano[1], Y. Fujihara[1], J. Zhang[1], T. Suzuki[2] and H. Suematsu[2]

Department of JMTR, Japan Atomic Energy Agency
[1]Institute for Integrated Radiation and Nuclear Science, Kyoto University
[2]Graduate School of Engineering, Nagaoka University of Technology

INTRODUCTION: The research and development (R&D) has been carried out for the production of Molybdenum-99 (^{99}Mo) by the neutron activation method ((n, γ) method) from viewpoints of limited availability of high-enriched uranium, no-proliferation and nuclear security, and disposal of nuclear fissile materials. It is essential to improve the properties of Alumina (Al_2O_3) used widely as Mo adsorbent for the $^{99}Mo/^{99m}Tc$ generator. In this study, four kinds of Al_2O_3 specimens[1] were prepared, and molybdenum adsorption and technetium-99m (^{99m}Tc) elution properties of these Al_2O_3 specimens were evaluated. Three kinds of MoO_3 pellets with different ^{98}Mo enrichment rations were also irradiated and evaluated the ^{99}Mo production amounts.

EXPERIMENTS: The MoO_3 pellets were fabricated by the cold pressing and sintering Method. Density of MoO_3 pellets was about 60%T.D. The MoO_3 pellet pieces (about 1.5 g) were irradiated in the Pn-2 of the KUR for 20 min. After the irradiation tests, the irradiated MoO_3 pellet pieces were dissolved with 6M-NaOH solution. Then, the Mo adsorption tests of the Al_2O_3 specimens were carried out with the sodium molybdate solution (10mg-Mo/mL, pH4) at RT. After the tests, each Al_2O_3 specimen adsorbing Mo was packed in the polypropylene column. The saline was flowed through in this column about every 24 h and the ^{99m}Tc was eluted from each Al_2O_3 specimen.

Three kinds of MoO_3 pellets with different ^{98}Mo enrichment ratios (>98.5%, 58.82% and natural isotope ratio (24.13%)) were prepared and irradiated in the Pn-2 of the KUR for 20 min. The activities of ^{99}Mo and ^{99m}Tc in the solution were measured by the γ-ray spectrometer.

RESULTS: Table 1 shows the result of ^{99}Mo adsorption amounts of Al_2O_3 specimens and ^{99m}Tc elution rates from Al_2O_3 specimens. The Mo adsorption amounts of the 3 types of developed Al_2O_3 (D-201-300, V-V-300, V-B-300) exceeded the medical alumina used in current commercial generators. The ^{99m}Tc elution rate was higher in the order of V-V-300, Medical, V-B-300, D-201-300. The ^{99m}Tc elution rate of V-B-300, that the Mo adsorption amount is the largest, was about 80% in 3 mL and the obtained ^{99m}Tc specific radioactivity was also highest as compared with other Al_2O_3 specimens. The Mo desorption rate was dependent on the ^{99m}Tc elution rate.

Table 2 shows the result of ^{99}Mo production amounts of MoO_3 pellets with different ^{98}Mo enrichment ratios. The ^{98}Mo enrichment ratios were re-evaluated from the results of the ^{99}Mo production ratio. The enrichment ratio of MoO_3 pellet with 58.82% was almost the same value as the measurement results. On the other hand, the experimental value was small in the enrichment ratio of MoO_3 pellet with >98.5%. After dissolution of the enrichment ratio of MoO_3 pellet with >98.5%, a white precipitate was observed in the solution and it is considered that the result was affected. In future, the experimental methods should be considered for the high accuracy results.

Table 1 Results of ^{99}Mo adsorption amounts of Al_2O_3 specimens and ^{99m}Tc elution rates from Al_2O_3 specimens

Items	^{99}Mo adsorption amounts		^{99m}Tc elution rates at 3 mL in Milking (%)		
	(MBq/g-Al_2O_3)	(mg-Mo/g-Al_2O_3)	1st run	2nd run	3rd run
Specimen-1 (D-201-300)	0.91	57.4	65.3	69.1	72.7
Specimen-2 (V-V-300)	0.88	55.4	92.4	91.2	91.1
Specimen-3 (V-B-300)	1.44	88.8	79.1	78.1	79.6
Specimen-4 (Medical)	0.63	39.0	89.4	83.3	83.6

Table 2 ^{99}Mo production amounts of MoO_3 pellets with different ^{98}Mo enrichment ratios

Enrichment ratio of ^{98}Mo	^{99}Mo production amounts (MBq/g-MoO_3)		Evaluation of ^{98}Mo enrichment ratio * (%)	
	Run 1	Run 2	Run 1	Run 2
> 98.5%	91.1	-	91.29	-
58.82%	56.3	57.4	51.17	60.87
Natural (24.13%)	26.5	22.7	(24.13)	(24.13)

* Based on specific radioactivity of natural abundance (24.13%)

CONCLUSION: The MoO_3 pellets were irradiated in the Pn-2 at KUR, and ^{99}Mo adsorption/^{99m}Tc elution properties of the Al_2O_3 specimens were evaluated with the solution of the irradiated MoO_3 pellets. As a result, it was suggested that V-B-300 could be used as Mo adsorbent for $^{99}Mo/^{99m}Tc$ generators using the (n, γ) method. However, in order to apply it to the generators, further improvement such as suppressing Mo desorption amount is required. It confirmed that ^{99}Mo production amounts increased with ^{98}Mo enrichment ratio and it is necessary to establish an evaluation method to improve the accuracy.

REFERENCES:

[1] Y. Suzuki *et al.*, Transactions of the Materials Research Society of Japan, **43** (2018) 75-80.

CO4-3 Precise Solution Stucture of Artificial Molecular Self-Assemblies in Water

N. Sato, K. Morishima, M. Sugiyama, Y.-Y. Zhan[1] and S. Hiraoka[1]

Institute for Integrated Radiation and Nuclear Science, Kyoto University
[1]Department of Basic Science, The University of Tokyo

INTRODUCTION: Binding of negatively charged species i.e. anions is one of the modern issues in molecular sciences, because binding of anions as well as cations has often seen in regulation and signal transduction in biological systems. Although artificial molecular hosts that bind cations have widely been developed so far, the progress in design and synthesis of those for anions is slower than that for cations. Now a day, several artificial anion-hosts have been reported, most of which have several hydrogen bonding donors to make strong multi-point hydrogen bonding between these donor atoms in the host and anions. Considering that desolvation is needed to bind anions in the molecular host, anion recognition in water, which strongly solvates the anions, is a challenging issue in anion recognition, but the understanding of the binding of anions in water is most closely related to biological events.

Recently, we found that a discrete, cube-shaped molecular self-assembly i.e. nanocube, which is composed of six gear-shaped amphiphiles (GSAs), is assembled in water.[1] The driving forces of this molecular self-assembly are the hydrophobic effect, van der Waals interactions, and cation-π interactions.[2] The thermodynamic[1] and kinetic[3] stabilities of the nanocube can rationally be tuned by the introduction of the substituents in the GSA. Furthermore, the nanocube can encapsulate relatively hydrophobic anion(s) in the 1-nm-sized hydrophobic cavity in water.[4] As the GSA has two positive charges on the pyridinium rings, the nanocube is a polycationic well-defined particle with 2 nm in diameter, so one of the driving forces of the binding of the anions in the nanocube would be electrostatic attraction between the anions and the cationic nanocube. The binding of anions in the nanocube in water is simply expressed by the following equation.

$$\text{X@nanocube} + \text{A}\cdot\text{S} \rightleftarrows \text{A@nanocube} + \text{X} + \text{S} \quad (1)$$

where A, X, and S indicate anion, the molecule(s) that stay in the cavity of the nanocube before the encapsulation of the anion (A), and solvent molecules (H_2O), respectively. Although we determined the thermodynamic parameters for the binding of anions in the nanocube by ITC measurement,[4] in order to precisely interpret the binding phenomenon, what is/are filled in the cavity of the nanocube before the encapsulation of the anions. As the counter anion of the nanocube is Cl^-, it is highly probable that Cl^- and/or several water molecules is/are tapped in the cavity. Thus in this study, to clarify whether Cl^- or water molecules is/are filled in the nanocube, we planned to measure SAXS of an aqueous solution of the nanocube because the SAXS profile should be affected by what occupies the cavity of the nanocube.

EXPERIMENTS: SAXS profiles were measured with a laboratory SAXS instrument (Rigaku NANOPIX) installed at Institute for Integrated Radiation and Nuclear Science, Kyoto University. X-ray wavelength was 1.54 Å and the typical sample-to-detector distance was 350 and 95 mm. A sample of the nanocube was prepared by dissolving solid sample of GSA in Milli-Q water. The concentration of the nanocube was determined by UV spectroscopy to be 0.758 mg/mL before the SAXS measurements.

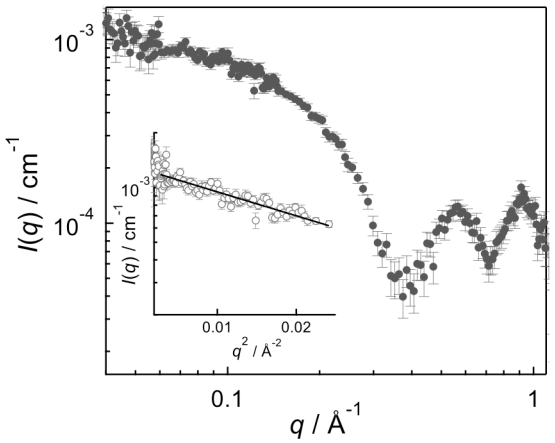

Fig. 1. A SAXS profile of a solution of **BM** nanocube in water. The inset shows the Guinier plot of the same data.

RESULTS: The SAXS profile and the Guinier plot for the nanocube are shown in Figure 1. It was found that the SAXS profile of the nanocube showed mainly two peaks, suggesting a discrete structure in water, which is consistent with the results obtained by other spectroscopic measurements, and that the discussion on the precise structure of the nanocube is possible based on the position and the intensity of the peaks. The radius of gyration (R_g) of the nanocube determined by the Guinier plot is 9.5 ± 0.4 Å, which is also consistent with the size of the nanocube determined by single-crystal X-ray analysis and ^{1}H DOSY spectroscopy. As it was confirmed that SAXS is powerful to discuss the precise solution structure of the nanocube, we are planning to investigate the change in the SAXS profiles by the encapsulation of several anions to conclude what are trapped in the cavity of the nanocube in water.

REFERENCES:

[1] Y.-Y. Zhan *et al.*, *Commun. Chem.*, **1** (2018) 14.
[2] Y.-Y.Zhan *et al.*, *Chem. Eur. J.*, **24** (2019) 9130–9135.
[3] Y.-Y. Zhan *et al.*, *Nature Commun.*, **10** (2019) 1414.
[4] Y.-Y. Zhan *et al.*, *Nature Commun.*, **9** (2018) 4530.

CO4-4

Correlation between Damage Accumulation by Neutron Irradiation and Hydrogen isotope Retention for Plasma Facing Materials

Y. Oya, M. Nakata, A. Koike, S. Yamazaki, T. Wada, M. Zhao[1], F. Sun[2], Y. Iinuma[3] and R. Okumura[3]

Graduate School of Integrated Science and Technology, Shizuoka University
[1]Graduate School of Science and Technology, Shizuoka University
[2]Faculty of Science, Shizuoka University
[3]Institute for Integrated Radiation and Nuclear Science, Kyoto University

INTRODUCTION: Due to the higher melting point and lower sputtering yield, tungsten (W) is considered as a candidate for plasma facing materials (PFMs) in the future fusion reactors. During the operation, W will be exposed to 14 MeV neutrons produced by D-T fusion reaction, as well as energetic particles such as hydrogen isotope, helium ion and charge-exchanged particles. The damages introduced by charge-exchanged particles are concentrated near the surface region, while that induced by 14 MeV neutrons are extended throughout the bulk. For the development of the effective fuel recycling and the safety operation, it is necessary to clarify the hydrogen isotope retention behavior in W with the consideration of damage distribution. In this study, irradiation damages were introduced by both of neutron and 6 MeV Fe ion irradiation with various damage distributions, and the D retention behaviors were evaluated by thermal desorption spectroscopy (TDS).

EXPERIMENTS: A disk-type polycrystalline W (6 $mm^{\varphi} \times 0.5\ mm^{t}$) purchased from A.L.M.T. Co. Ltd. was used. To remove impurities and damages introduced during the polishing processes, the samples were heat-treated at 1173 K under ultrahigh vacuum (< 10^{-6} Pa). Thereafter, the samples were damaged by 6 MeV Fe^{2+} irradiations at room temperature with the damage concentrations of 0.01–0.1 dpa (displacement per atom) by a 3 MV tandem accelerator in Takasaki Ion Accelerators for Advanced Radiation Application (TIARA) at National Institutes for Quantum and Radiological Science and Technology (QST), and the fission neutron irradiations under 323 K by Kyoto University Research Reactor Institute (KUR) with the damage concentration up to 0.015 dpa. After the damage irradiation, the 1.0 keV deuterium ion (D_2^+) implantation was performed on the W sample at Shizuoka University. The D ion fluence was set to be 1.0×10^{22} D^+ m^{-2} with the ion flux of 1.0×10^{18} D^+ m^{-2} s^{-1}. The D desorption behavior was evaluated by TDS at the temperature up to 1173 K with the heating rate of 0.5 K s^{-1}.

RESULTS: Fig. 1 shows D_2 TDS spectra for neutron - Fe^{2+} damaged W samples with various damage distributions. For the comparison, D_2 TDS spectra for only Fe^{2+} damaged samples are shown in Fig. 2. The D_2 TDS spectra were assumed to consist of four major D desorption

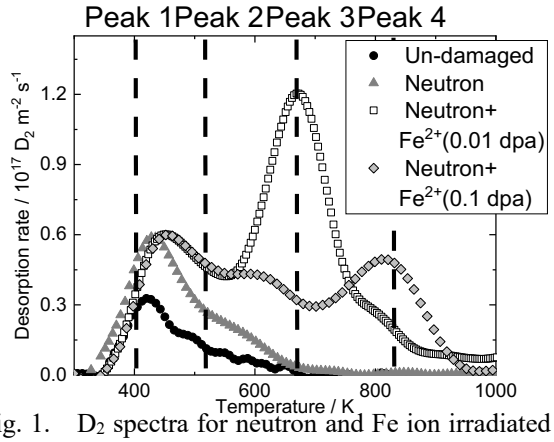

Fig. 1. D_2 spectra for neutron and Fe ion irradiated samples with various damage concentrations

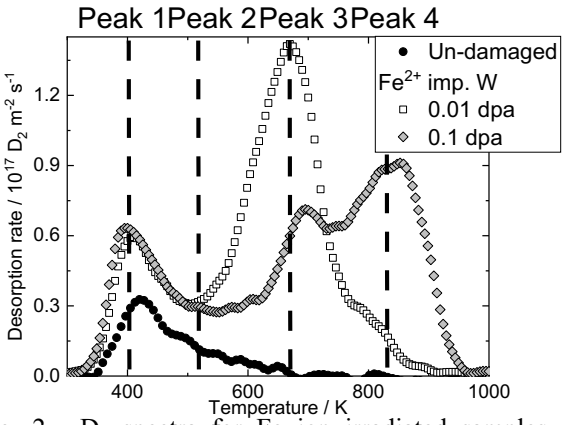

Fig. 2. D_2 spectra for Fe ion irradiated samples with various damage concentrations

stages located at 400 K, 550 K, 650 K and 850 K, respectively. Based on our previous studies, the D desorption stages at Peaks 1 to 4 were corresponded to the desorption of D adsorbed on the sample surface or trapped by dislocation loops, vacancies, vacancy clusters and voids, respectively [1]. In the neutron irradiated sample, D was adsorbed on the surface and/or trapped by dislocation loops and vacancies. The D retentions at Peaks 3 and 4 for multiple neutron - Fe^{2+} damaged W were decreased by neutron irradiation, as shown in Figs. 1, 2. In our previous report [1, 2], the hydrogen isotope recycling was enhanced by the dense damage introduction in the shallow region, and the damages would suppress D diffusion according to the result of HIDT simulation. It was considered that the D diffusion was limited by the increase of point defects by neutron irradiation. It was concluded that total D retention was decreased in the multiple neutron - Fe^{2+} irradiated samples.

REFERENCES:

[1] H. Fujita, K. Yuyama, X. Li, *et al.,* Phys. Scr. **T167** (2016) 014068.
[2] M. Nakata, K. Azuma, A. Togari, *et al.,* Fusion Engineering and Design, In press.

CO4-5 Electron Emission Properties of Field Emitter Array for Image Sensor under Gamma-ray Irradiation

Y. Gotoh, T. Morito, M. Nagao[1], T. Okamoto[2], N. Sato[3], M. Akiyoshi[4] and I. Takagi

Graduate School of Engineering, Kyoto University

[1]*National Institute of Advanced Industrial Science and Technology*

[2]*Naational Institute of Technology, Kisarazu College*

[3]*Institute for Integrated Radiation and Nuclear Science Kyoto University*

[4]*Radiation Reactor Center, Osaka Prefecture University*

INTRODUCTION: We have been developing a radiation tolerant vacuum-type image sensor [1]. The image sensor consists of a matrix-driven field emitter array (FEA) and a photoconductor. It has already been proven that the FEAs have sufficient radiation tolerance against cobalt 60 gamma-rays, up to 1.2 MGy [2]. Following this result, operation of the FEAs under gamma-ray irradiation was conducted last year, with a small vessel that can maintain the pressure at 10^{-6} Pa with an aid of non-evaporation getter (NEG) pump [3]. The FEA and the anode made of stainless steel was set into a glass tube, but it was difficult to realize an image sensor configuration due to a small space. In this study, the vessel was re-made to realize a vacuum image sensor.

EXPERIMENTS: The image sensor could be realized by setting the FEA, mesh electrode, and the photoconductor on a base flange with the size of ICF152. The holder of the FEA was made of machinable ceramics. Unlike the previous vessel, the light or the image could be introduced through a view-port. The vacuum gauge could be mounted on the vessel to monitor the pressure of the vessel. The NEG pump adopted in the present study was the same one with the previous report [3]. Prior to the exposure to gamma-ray, the pressure of the vessel with an NEG pomp activated was recorded, and the vessel maintained the pressure less than 10^{-6} Pa for about 10 days. At the practical test, the pressure was about 1.2 x 10^{-6} Pa. The FEA tested in this study was a matrix-type single-gated Spindt-type with 1024 emission tips. The emitter material was nickel. Before the measurements under irradiation, sufficient aging was performed prior to the exposure to gamma-ray. The measurements of the electron emission property of the FEA was performed at Co-60 Gamma-ray Irradiation Facility, Institute for Integrated Radiation and Nuclear Science, Kyoto University. The dose rate of irradiation was roughly estimated to be 1.3 kGy h^{-1}.

RESULTS: Among the 168 FEAs fabricated on the present sample, one of them that located at the center of the sample was chosen. The electron emission property was measured with the following parameters: gate voltage of 30 V for the selected gate but 0 V for the other, anode voltage of 200 V, gate series resistor of 1 MΩ, emitter series resistor of 1 MΩ. For the selected emitter, a ramp voltage or a constant voltage was applied to observe the variation of the properties under the gamma-ray irradiation. Figure 1 shows the variation of the anode current with and without gamma-ray irradiation. No significant change was observed between with and without gamma-ray irradiation.

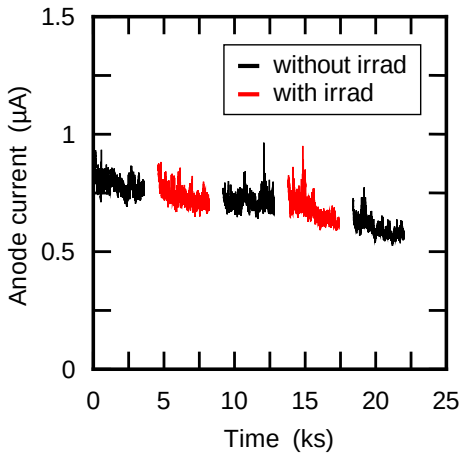

Fig. 1. Variation of the anode current with and without the gamma-ray irradiation.

Detailed analysis of the electron emission was performed with the Seppen-Katamuki analysis which was developed by the authors to evaluate the field emitters [4]. This method enables us to evaluate the surface state (mostly work function) even though the deviation in electron emission. The results suggested that the surface state did not vary even under the gamma-ray irradiation. However, a separate experiment showed a possible changes of surface microstructure of the emitter, which results in the step noise of the anode current.

ACKNOWLEDGMENTS: The present study was partially supported by Japan Society for the Promotion of Science, through a Grant-in-Aid for Scientific Research, KAKENHI 16H04631 and also by Futaba Electronics Memorial Foundation.

REFERENCES:

[1] Y. Gotoh *et al.,* IEEE 28th International Vacuum Nanoelectronics Conference (2015) p. 240.
[2] Y. Gotoh *et al.*. IEEE 29th International Vacuum Nanoelectronics Conference (2016) p. 20.
[3] Y. Gotoh *et al.,* KURRI Progress Report 2017 (2017).
[4] Y. Gotoh *et al.,* J. Appl. Phys. **121** (2017) 234503.

CO4-6 Neutron Irradiation to Liquid Breeders for Fusion Reactors and Tritium Recovery

S. Fukada, K. Tsukahara, Y. Iinuma[1], K. Katayama, M. Oya

Interdisciplinary Graduate School of Engineering Sciences, Kyushu University
[1]KURNS, Kyoto University

INTRODUCTION: Liquid blanket materials such as Li liquid metal, $Li_{17}Pb_{83}$ eutectic alloy or $LiNaBeF_4$ (Flinabe) molten salt are expected to work for a tritium breeding material through the $^6Li(n,\alpha)^3T$ reaction in D-T fusion reactors. These liquid breeding materials have appropriate properties of high Li density necessary for the high tritium breeding ratio, good thermal conductivity for high heat transfer and high γ -ray shielding in fusion reactor blankets. However, there were few experimental studies of tritium recovery from liquid blanket materials using neutron irradiation facility [1-5]. In the present study, tritium recovery from liquid Li or molten Flinabe after neutron irradiation is demonstrated experimentally. In case of the Li breeder, tritium equilibrium pressure is extremely low because of high tritium affinity to Li, which is estimated as $2.2x10^{-9}$ Pa at T/Li=$1x10^{-6}$ in atomic ratio and 500°C. Yttrium metal is selected to work for a tritium recovery material from the Li blanket. On the other hand, tritium (TF) in Flinabe is recovered by the isotopic exchange reaction of $TF + H_2 \rightarrow HT + HF$.

EXPERIMENTS: Li and Flinabe were selected as the tritium breeder for neutron irradiation through the pneumatic facility (pn-2) in KUR having thermal power of 5 MW. One gram of Li or Flinabe is irradiated under the conditions of the neutron flux $2.75x10^{13}$ n/cm^{2}s and irradiation time of one minute. Samples were remained in glovebox for one month to decrease radioactivity of radio nuclides, which have short decay time of ^8Li ($\tau_{1/2}$=0.84 s) or ^{24}Na ($\tau_{1/2}$=15 hr). Irradiated Li samples were contacted with Y metal tips at 300°C in a reaction chamber for specified time. Li is contacted with metallic Y tips shown by Photo 1 and tritium is distributed between Li and Y. Tritium activities in Li and Y are measured by using the two chemical dissolution reactions of $2LiT_X + H_2O \rightarrow Li_2O + 2xHT + (1-x)H_2$ and $YT_X + HNO_3 \rightarrow Y(NO_3)_3 + xHT + ((3-x)/2)H_2$. HT released in purge Ar gas is converted to HTO by a CuO particles bed, and a liquid scintillation counter is used for tritium detection.

RESULTS: Fig. 2 shows the recovery ratio of tritium from Li to Y. When Y surfaces are treated by HF solution before contact with Li and Y, the recovery rate is enhanced. This is because surfaces of Y metal tip without HF treatment are oxidized and it affairs tritium diffusion into metal bulk. So, the Y oxides are removed by HF solution. Its surfaces are converted to YF_3. Tritium in Li is correlated by the first-order reaction rate equation regardless of HF treatment of not.

Photo 1 Overview of Y Tips for T recovery from Li.

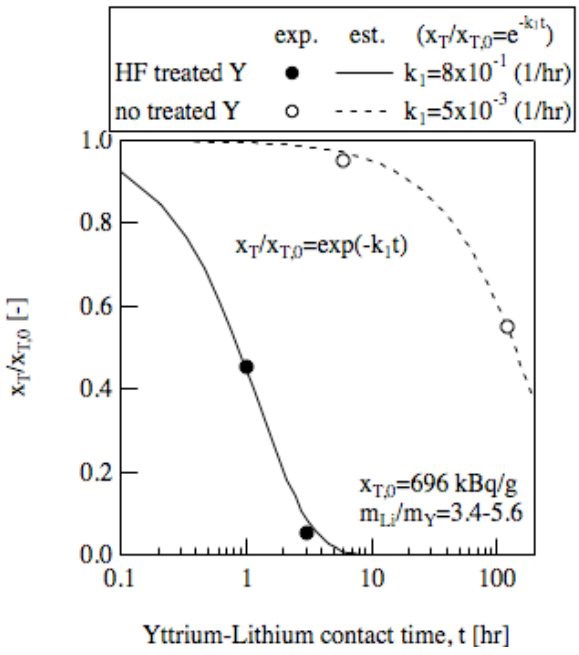

Fig. 2 Tritium recovery ratio from neutron irradiated Li by Y metal tips at 300°C.

REFERENCES:

[1] Y. Yamasaki, S. Fukada, K. Hiyane and K. Katayama, Fusion Science and Technology, 71(4) (2017) 501-506.
[2] S. Fukada, T. Nishikawa, M. Kinjo and K. Katayama, Fusion Engineering and Design, 135 (2018) 74-80.
[3] K. Hiyane, S. Fukada, Y. Yamasaki, K. Katayama and E. Wakai, Fusion Engineering and Design, 109-111 (2016) 1340-1344.
[4] K. Kumagai, T. Tanaka, T. Nagasaka, J. Yagi, T. Watanabe, G. Yamazaki, F. Sato, S. Tamaki, I. Murata, S. Fukada, K. Katayama and A. Sagara, Plasma and Fusion Research, 14 (2019) 1405044.
[5] J. Yamashita, R. Nishiumi, S. Fukada, K. Katayama, A. Sagara and J. Yagi, Fusion Engineering and Design, 136 (2018) 173-177.

CO4-7 Damage Evolution in Neutron-irradiated Metals during Neutron Irradiation at Elevated Temperatures

I. Mukouda and Q. Xu[1]

Hiroshima International University
[1]Institute for Integrated Radiation and Nuclear Science, Kyoto University

INTRODUCTION: It is accumulated an attention that a damage structure in neutron irradiated metals differs if the temperature is varied during irradiation [1]. Especially effect of lower temperature irradiation on the development of damage structure in metals which are irradiated subsequently at higher temperature was reported to be remarkable because the point defects nucleate at lower temperature more frequently during an irradiation. Recently the temperature controlled irradiation devices were developed at KUR [2]. It becomes possible to irradiate continuously at two stage of temperature. In the present work, effects on damage formation in neutron-irradiated copper for the temperature variation were examined for an irradiation at low fluence regime.

EXPERIMENTS: Copper disks of 3mm in diameter were prepared with 99.999% nominal purity specimen. Before an irradiation, they were annealed for 5 hours at 1273 K in vacuum of 10^{-5} Pa. Specimens were irradiated by fission neutrons in a temperature controlled irradiation device in KUR-SSS. In the previous temperature varying irradiation, specimens were irradiated at first at 473 K for 10 hours and subsequently at 573K for 10 and 20 hours at 5MW. After a radiation cooling, they were observed by electron microscopy. A TEM observation was carried out using g = (002) reflection with (g, 5g) condition for the specimens of (110) configuration. Voids were observed in a bright field image by taking a slightly under forcussed image. A triangular image was taken as stacking fault tetrahedra (SFT) and diffused dot image was tentatively taken to be an interstitial cluster.
Present temperature varying irradiation, specimens were irradiated at 473K-6hrs/573K-40hrs and 473K-23 hrs/573K-23 hrs at 1MW. TEM observation are carried out recently.

RESULTS: In 473K-10hrs/573K-10hrs irradiation at 5MW, the number density of voids and SFT was smaller than those of constant temperature irradiation at 573K. Especially the decrease of number density of voids was significant as shown in Figure 1. Fig. 1(a) shows dislocations in the specimen. Dislocations were not decorated by interstitial clusters. Fig. 1(b) shows point defects clusters. The number density of SFT was smaller than the value in copper which were irradiated at constant temperature of 573 K. Only one void was observed in specimens as in this picture, which means the formation of voids was suppressed significantly by the present temperature elevation irradiation.
Neutron-irradiated copper at 573K for 10 hours at 5MW, the dislocation structure show no decorated interstitial clusters around dislocation. Interstitial clusters, which were accumulated along dislocation lines, were unified to grow to dislocations. This makes development of complicated structure of dislocations as reported by Mukouda and Shimomura [3].
The suppression of void formation in temperature-varied irradiation suggests that the nucleation of voids during a constant temperature irradiation at 573K in copper occurs during the period of dislocation decoration by interstitial clusters. Detail consideration are progress by lower irradiation dose at 1MW.

REFERENCES:
[1] N. Yoshida, Q. Xu, H. Watanabe, Y. Miyamoto and T. Muroga, J. Nucl. Mater., 212-215 (1994) 471.
[2] T. Yoshiie, Annual Reports of KUR (1998).
[3] I. Mukouda and Y. Shimomura, Material Science & Engineering A309-310 (2001) 190-197.

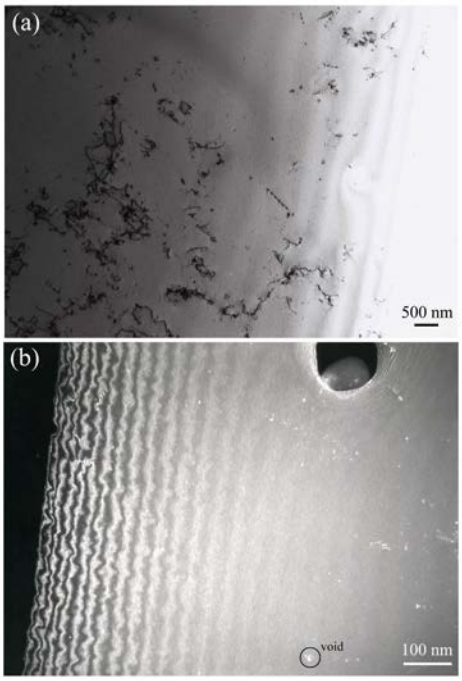

Fig. 1. Damages observed in neutron-irradiated copper with temperature varying schedule. The irradiation was carried out at first at 473K for 10 hours and subsequently at 573 K for 10 hours.

CO4-8 The correlation between microstructural evolution and mechanical property changes in neutron-irradiated vanadium alloys

K. Fukumoto[1] and Xu Qiu[2]

[1] *RINE, Univ. of Fukui*
[2] *KURNS, Kyoto Univ.*

INTRODUCTION: In order to understand the thermal stability of defect clusters, and investigate a recovery method for irradiation hardening and embrittlement, post-irradiation annealing experiments are performed to evaluate the recovery of microstructure and mechanical properties of vanadium alloys irradiated below 300°C.
In this study, experiments to determine the influence of post-irradiation annealing on mechanical properties and microstructures in neutron-irradiated V-Cr-Ti alloys are described. Two groups of specimens (as-irradiated specimens and specimens which underwent the post-irradiation annealing treatment) were subjected to tensile tests at room temperature and 500°C. Post-irradiation annealing experiments with long intervals of up to 50 hr were used to recover the original strength and ductility.

EXPERIMENTS: The majority of test specimens for this study were prepared from V-4Cr-4Ti alloys. The tensile specimens had nominal gauge dimensions of 0.25mm(t) x 1.2mm(w) x 5mm(l). Before irradiation, all specimens were annealed in vacuum at 1000°C for 2hrs. The specimens were irradiated at 228°C to 280°C with 3 to 5 displacements per atom (dpa) in the ATR-A1 or at 306°C with 6 dpa in the HFIR-11J. Post-irradiation annealing was carried out for 2 to 50 hr at 500°C and 600°C in a vacuum. Tensile tests were conducted at room temperature and 500°C. TEM samples were punched from non-deformed areas of tested specimens. The microstructural TEM observations were performed in KUR/Kyoto Univ.

RESULTS: As-irradiated V-4Cr-4Ti alloys in ATR-A1 and HFIR-11J showed the reduction of ductility below 1% and remarkable irradiation hardening above 700MPa in RT tensile tests. A recovery of ductility to 3% and hardening to 500MPa could be observed in an annealed V-4Cr-4Ti alloy at 600°C for 2hrs. On the other hand, no typical changes in uniform elongation and yield stress increase could be seen in an annealed one at 500°C for 2hrs in tensile test. The V-4Cr-4Ti alloys annealed at 500°C for 20hrs showed no change of yield stress increase compared to as-irradiated one in the tensile test at RT, but the total elongation was recovered to 5% with the stress-strain curve like complete elasto-plastic behavior. Even at 500°C tensile test, recovery of ductility could be seen in annealed sample at 500°C for 20hrs. In the case of annealed sample for 50hrs, the ultimate tensile strength decreased significantly with 5% of uniform elongation.
Figure 1 shows the changes in the damage microstructure of V-4Cr-4Ti for different post-irradiation annealing times. In the as-irradiated specimens, the density of defect clusters was very high and the size of each cluster was very small (i.e., about a few nm). With increasing annealing time at 773K, the density of defect clusters decreased gradually. After annealing for 50 h at 773K, the clusters grew into large dislocation loops. Those large loops were identified as dislocations with a/2<111> Burgers vector. No Ti(OCN) precipitates could be seen on {100} habit plane in the as-irradiated and annealed V-4Cr-4Ti alloys. Figure 5 shows the effects of annealing time on the density and average size of the defect clusters and dislocation loops in the post-irradiation annealed V-4Cr-4Ti alloys. With increasing annealing time, the density of defect clusters decreased and the defect clusters grew into dislocation loops. It was found that the recovery of mechanical behavior can be appeared after 10 hour anneal at 500C in order to improve the low-temperature irradiation embrittlement behavior of V-4Cr-4Ti alloys.

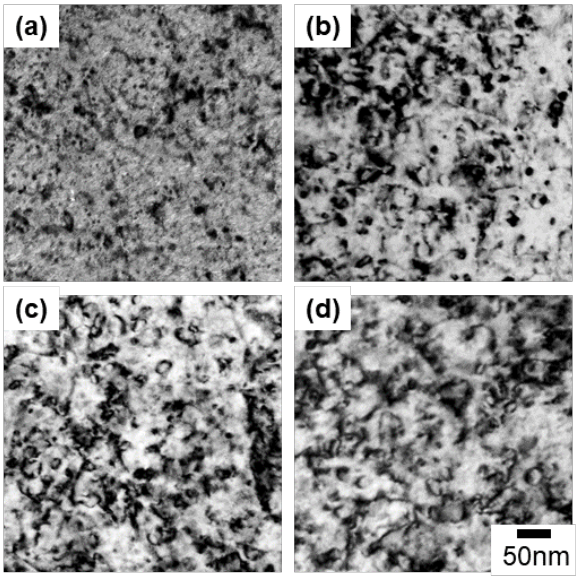

Fig.1. A set of transmission electron micrographs of as-irradiated and post-irradiation annealed V-4Cr-4Ti alloys: (a) as-irradiated, (b) 10 h annealed, (c) 20 h annealed, (d) 50 h annealed.

CO4-9 Search of materials forming nano-porous structures by high-energy ion irradiation and study on its formation mechanisms

J. Yanagisawa, Q. Xu[1], A. Yabuuchi[1], K. Takamiya[1], and A. Kinomura[1]

School of Engineering, The University of Shiga Prefecture
[1]*Institute for Integrated Radiation and Nuclear Science, Kyoto University*

INTRODUCTION: We have been reported that the formation of porous structures with nanometer size (nano-porous structures) can be formed on Ge surfaces by high-energy (100-200 keV) Ga, Au or Si ion irradiations, but no such structures were formed by low-energy (15-30 keV) Au or Si ion irradiations [1]. Last year, large-area ion irradiations on Ge surfaces with 60 keV Ar ions were performed at Research Reactor Institute, Kyoto University, and the formation of nano-structures were confirmed using such ion irradiation conditions [2]. In the present study, lower-energy Ar ion irradiation was performed and the S (line shape) parameters of the positron annihilation was measured as a function of the positron energy to confirm the formation mechanisms of such nano-structures in an early stage by ion irradiation.

EXPERIMENTS: After cleaning of Ge(110) chip samples with an area of about 1.5 x 1.5 cm^2, a corner part of each sample was covered with aluminum foil to prevent the ion irradiation. Three kind of samples were prepared by the Ar ion irradiations using the different ion energy and total fluence, that is, 50 keV and 5 x 10^{16} cm^{-2}, 25 keV and 1 x 10^{16} cm^{-2}, and 50 keV and 1 x 10^{16} cm^{-2}, respectively. S parameters was obtained from the Doppler broadening of annihilation gamma-rays as a function of incident positron energy by the KUR slow positron beam system.

RESULTS and DISCUSSION: Figure 1 shows the optical microscope images of the sample surfaces. It is found that the ion irradiated region was changed to dark, indicating that the formation of nano-structures on the Ge surfaces was confirmed even after such lower ion energy irradiations.

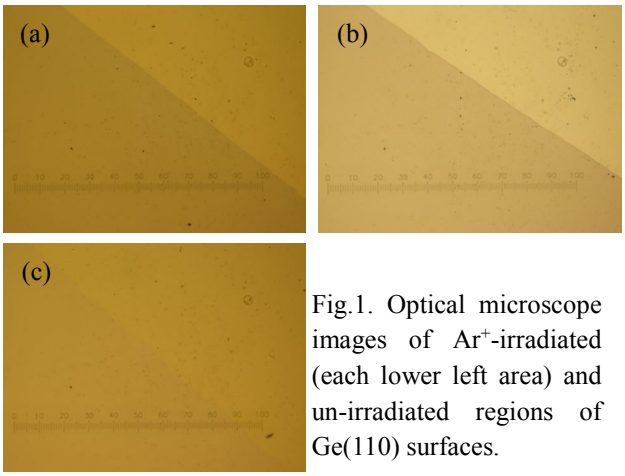

Fig.1. Optical microscope images of Ar^+-irradiated (each lower left area) and un-irradiated regions of Ge(110) surfaces.
(a) 50 keV, 5x10^{16} cm^{-2}, (b) 25 keV, 1x10^{16} cm^{-2}, and (c) 50 keV, 1x10^{16} cm^{-2}.

Figure 2 shows the S parameters for the ion-irradiated and un-irradiated Ge samples plotted as a function of incident positron energy. VEPFIT code was used for the fitting in the figure. After Ar ion irradiation, S parameters were increased compared to the un-irradiated sample. For the samples with the same ion fluence of 1x10^{16} cm^{-2}, the increase in S parameter for the sample with the ion irradiation energy of 50 keV (solid diamonds in Fig. 2) was larger than that of 25 keV (solid squares), indicating that the total amount of the atomic vacancies and/or voids induced by the ion irradiation becomes larger for higher ion energy irradiation. On the other hand, dependence of the ion fluence on the S parameter was not observed for the 50 keV-Ar-ion irradiation (solid triangles and diamonds in Fig. 2).

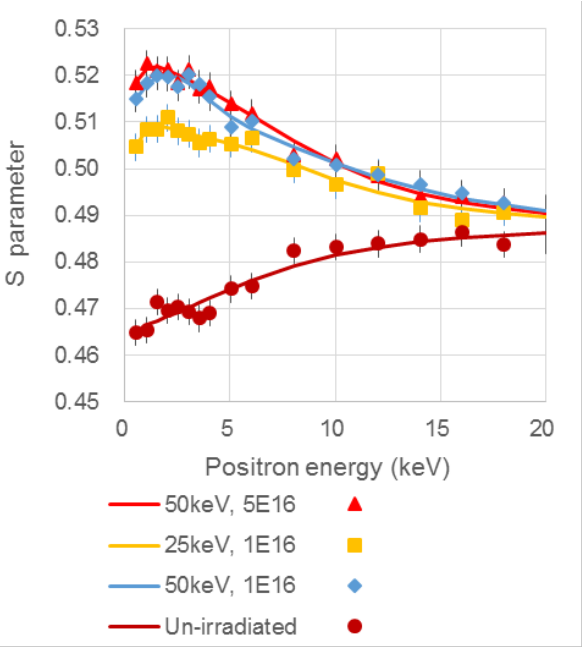

Fig.2. S parameters for Ar^+-irradiated and un-irradiated Ge(110) samples as a function of positron energy.

CONCLUSION: Effect of the low-energy Ar ion irradiation on Ge (110) surfaces was studied using S parameters of the slow positron beam measurements. It is confirmed that the atomic vacancies and/or voids formed inside the surface region increase with increasing the ion energy. Further discussion, such as the influence of the ion fluence and the size and distribution of voids, is an issue in the future.

REFERENCES:

[1] J. Yanagisawa, K. Takarabe, K. Ogushi, K. Gamo and Y. Akasaka, J. Phys.: Condens. Matter **19** (2007) 445002 (10pp).
[2] J. Yanagisawa, Q. Xu, A. Yabuuchi, K. Takamiya, and A. Kinomura, KURRI Progress Report 2017 (Kyoto University), 129 (CO4-15, 29061).

CO4-10 Irradiation Experiment of Accident Tolerant Control Rod Materials

H. Ohta[1], Y. Nauchi[1], K. Nakamura[1] and T. Sano[2*],
H. Unesaki[2]

[1]*Nuclear Research Technology Laboratory, Central Research Institute of Electric Power Industry*
[2]*Institute for Integrated Radiation and Nuclear Science, Kyoto University*
[*]*Present affiliation: Atomic Energy Research Institute, Kindai University*

INTRODUCTION: To improve the safety of light water reactors (LWRs) against severe accidents (SAs), various concepts of "enhanced-accident tolerant fuels and core components" are developed in many countries. The Central Research Institute of Electric Power Industry (CRIEPI) has been developing an accident tolerant control rod (ATCR) to which the novel neutron absorbing materials including rare-earth sesquioxides (RE_2O_3) are applied[1], since current control rods using Ag-In-Cd alloy or B_4C may be damaged and removed from the core in early stage of SAs before serious fuel rod failure occurs. The ATCR improves the reactor shutdown margin and neutronic lifetime, as well as reduces the risk of re-criticality accident in any reactor conditions. For the ATCR candidate materials RE_2O_3-MO_2 (RE = Sm or Eu, M = Zr or Hf), a high temperature compatibility with steel, which is a control rod cladding material, and physicochemical stability under high temperature steam atmosphere were experimentally confirmed so far[2]. Furthermore, a reactivity analysis in representative LWRs indicated that these candidate materials have enough reactivity worth comparable to or higher than the conventional neutron absorbing materials Ag-In-Cd alloy or B_4C[3]. In addition, thermal neutron irradiation characteristics of these candidate materials are needed to be confirmed to evaluate the applicability as a control rod for LWRs. In this study, dimensional stability of a candidate material by neutron irradiation will be confirmed.

SAMPLE PREPARATION: The powders of Sm_2O_3 and ZrO_2 were mixed at a molar ratio of 1 : 1 and sintered to form a pellet with a diameter of 8.1 mm and a height of 8.1 mm as shown in Fig. 1. The pellet density was measured to be 6.55 g/cm^3 corresponding to 93.7 % of the theoretical density. Sintered Sm_2O_3-ZrO_2 mixture with a molar ratio of 1 : 1 is known to form a fluorite crystal structure and its long-term stability in water or steam has been confirmed by previous study[1]. Since Sm_2O_3-HfO_2, Eu_2O_3-ZrO_2 and Eu_2O_3-HfO_2 also have the same fluorite crystal structure as Sm_2O_3-ZrO_2, the results of this irradiation experiment are expected to be applicable to the other candidate materials. For the purpose of minimizing the radioactivation induced by the neutron irradiation, the sintered pellet was cut into small pieces.

Fig. 1 Sm_2O_3-ZrO_2 pellet.

The appearance of the cut sample pieces was observed with an optical microscope and measured the external dimensions, as shown in Fig. 2. Major specifications of the samples prepared for the irradiation experiment are summarized in Table I.

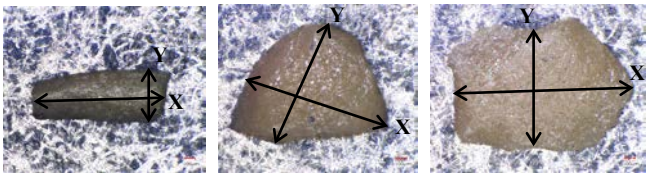

(1) (2) (3)

Fig. 2 Appearance of irradiation samples of Sm_2O_3-ZrO_2.

Table I. Irradiation Sample Specifications

	(1)	(2)	(3)
Composition	Sm_2O_3-ZrO_2	←	←
Density	93.7%TD	←	←
Weight	1.95mg	6.21 mg	5.15 mg
External dimension			
X direction*	1.397mm	1.569mm	1.851mm
Y direction*	0.562mm	1.371mm	1.236mm

*: See Fig. 2.

EXPERIMENTS: Irradiation experiment has been carried out from 11/27/2018 to 02/14/2019 using long-term irradiation plug in Kyoto University Research Reactor (KUR). The above three samples were enclosed in an Al capsule dedicated for long-term irradiation experiment and irradiated for 259 hours at a rated power of 1 MW and 45 hours at a high power of 5 MW. It is estimated that the thermal and epithermal neutron fluences at the end of irradiation experiment are 1.69×10^{19} n/cm^2 and 5.96×10^{17} n/cm^2, respectively. Currently, the irradiated Sm_2O_3-ZrO_2 samples are cooled to reduce the radioactivity (3.23×10^{10} Bq) induced by the irradiation.

POSTIRRADIATION OBSERVATION PLAN: After appropriate cooling period, the appearances of the irradiated samples are observed and their external dimensions are precisely measured. Then, the weights of the samples are also measured to assess density changes during irradiation. Furthermore, the morphology of the sample surface is observed in detail with an electron microscope to confirm the irradiation damage. On the basis of these irradiation experiment and postirradiation observation results, applicability of RE_2O_3-MO_2 to control rod for LWRs will be discussed.

REFERENCES:

[1] H. Ohta, *et al.*, TopFuel 2016, 17556 (2016).
[2] K. Nakamura, *et al., AESJ 2017 spring meeting*, 1I06 in Japanese.
[3] H. Ohta, *et al., Trans. 2018 ANS winter meeting*, Vol. 119, pp425-428 (2018).

CO4-11 Valence change behavior of Cu ions in oxide glasses by γ-ray irradiation

R. Hashikawa, A. Kinomura[1], T. Saito[1], A. Okada[2], T. Wakasugi[2], K. Kadono[2]

Graduate School of Science and Technology, Kyoto Institute of Technology
[1]Institute for Integrated Radiation and Nuclear Science, Kyoto University
[2]Faculty of Materials Science and Engineering, Kyoto Institute of Technology.

INTRODUCTION: Exposure to high energy radiation generates electron-hole pair in glass. A part of the electrons and holes are captured by metal ions present in the glass, resulting in the change in valence of the metal ions. Using this phenomenon, new luminescent centers are generated in the glass. This is known as "Radiophotoluminescence (RPL)", which is applied to luminescent glass used for personal dosimeter [1]. The absorbed dose can measured from the luminescence intensity because it is proportional to the absorbed dose. We have reported that a Cu-doped glass exhibits RPL phenomenon and a well proportionality between the luminescence intensity and absorbed dose [2]. Here we carried out quantitative analyses for the relationship between the variation in the valence of copper ions, absorbed dose, and the RPL intensity.

EXPERIMENTS: Glass was prepared through a conventional melting-cooling method using reagent grade raw materials, $NaNO_3$, Al_2O_3, SiO_2, B_2O_3, and CuO. The glass composition is $25Na_2O \cdot 25Al_2O_3 \cdot 10B_2O_3 \cdot 40SiO_2$ (mol%) doped with CuO of 0.005 mol% for the 100 mol% glass. The prepared glass was cut to the size of 15 x 15 mm^2 and 1 mm in thickness. Gamma-ray irradiation experiments were performed with ^{60}Co γ-ray at the Co-60 Gamma-ray Irradiation Facility at Institute for Integrated Radiation and Nuclear Science, Kyoto University. The irradiation dose was represented as absorbed dose for water.

RESULTS: The mechanism proposed for the RPL phenomenon in the Cu-doped aluminoborosilicate glasses is considered to be as follows [2]. Copper in the glass mainly exists as divalent Cu^{2+} or monovalent Cu^+ ions. Although Cu^{2+} ions has no luminescence, Cu^+ ions has a bright one around 2.5 eV (500 nm) by excitation at 240 nm. A part of the electrons and holes generated in the glass by the high energy radiation are captured by the Cu^{2+} and Cu^+ ions, respectively.

$$\text{Glass} \rightarrow h^+ + e^-$$
$$Cu^{2+} + e^- \rightarrow Cu^+$$
$$Cu^+ + h^+ \rightarrow Cu^{2+}$$

Since the molar fraction of Cu^{2+} is larger than that of Cu^+ in the aluminoborosilicate glass, the electron-captured reaction is predominant. Therefore, the intensity of Cu^+ luminescence increases after the high energy irradiation.

Figure 1 shows the variation of absorption spectra of the Cu-doped aluminoborosilicate glass before and after the γ-ray irradiation. The inset shows the variation of the absorption band assigned to the d-d transition of Cu^{2+} ions. The intensity of the absorption band is decreased because the Cu^{2+} ions became Cu^+ by the capture of the electrons which are generated by the irradiation.

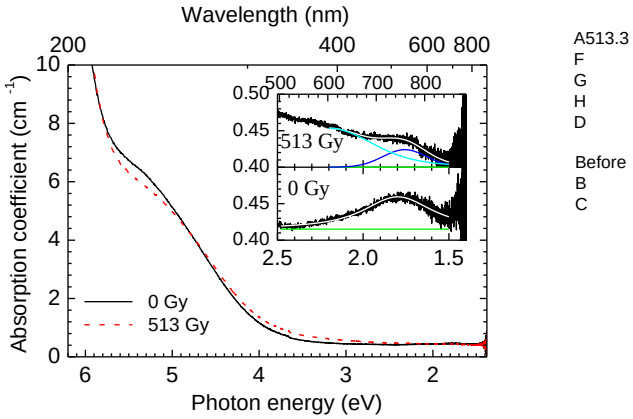

Fig. 1. Absorptions spectra of Cu-doped aluminoborosilicate glass before and after the γ-ray irradiation with the absorbed dose of 513 Gy

The dependences of the absorption and RPL intensities on the absorbed dose are presented in Fig. 2. Absorption and RPL intensities decreased and increased lineally with the absorbed does until about 800 Gy. This is well consistent with the RPL mechanism for the Cu-doped glass. The slop of the proportional line between the absorption intensity and the dose was -1.89×10^{-5} $cm^{-1} \cdot Gy^{-1}$. From this value and the molar absorption coefficient of Cu^{2+} in aluminoborosilicate glass, 26.9 $L \cdot mol \cdot cm^{-1}$ [3], 95 % of Cu in the glass existed as the divalent state, Cu^{2+}, before irradiation and the 0.041 % of Cu^{2+} was varied to Cu^+ ions per 1 Gy irradiation.

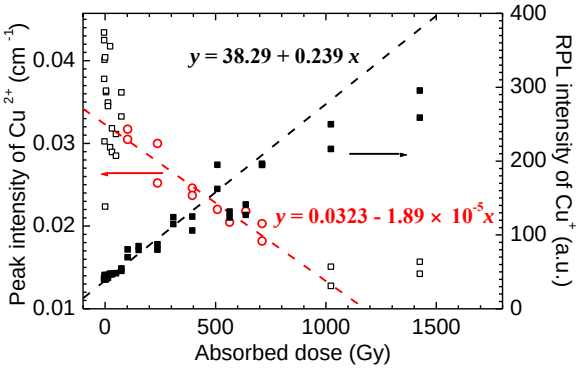

Fig. 2. Dependences of the intensities of the absorption band due to Cu^{2+} ions and RPL of Cu^+ on the absorbed dose.

REFERENCES:

[1] R. Yokota, *et al.*, J. Phys. Soc. Jpn., **23** (1966) 1038-1048.
[2] H. Hashikawa, *et al.*, J. Am. Cer. Soc., **102** (2019) 1642-1651.
[3] W. Thiemsorn, *et al.*, J. Solid Mech. Mater. Eng., **1** (2007) 508 - 518.

CO4-12 Elucidation of the Mechanism of the Solvent-dependent Helix Inversion of Polymer Main Chain Based on the Small Angle X-ray Scattering

Y. Nagata[1], M. Suginome[1], M. Sugiyama[2], R. Inoue[2], N. Sato[2], and K. Morishima[2]

[1] *Graduate School of Engendering, Kyoto University*
[2] *Institute for Integrated Radiation and Nuclear Science, Kyoto University*

INTRODUCTION: Much attention has been paid to the structural control of artificial helical polymers because of their potential applications for asymmetric catalysts, chiral stationary phase, and chiroptical materials. Recently, we found that single-handed helical poly(quinoxaline-2,3-diyl)s (PQXs) bearing chiral side chains exhibit a solvent-dependent helix inversion,[1-3] which can serve as effective scaffold for chirality-switchable materials. [4-7]

In order to elucidate the mechanism of the solvent-dependent helix inversion of PQXs, we have revealed detailed structures of a PWX with right- or left-handed structures in tetrahydrofran-d_8 (THF-d_8) or a mixed solvent of 1,1,2-trichloroethane-d_3 (1,1,2-TCE-d_3) and THF-d_8 (8/2, v/v) by using small-angle neutron scattering (SANS) experiments, in conjunction with theoretical calculations.[8] The obtained structures of the PQX suggested that the right-handed structure in THF-d_8 is well solvated, while the left-handed structure in 1,1,2-TCE-d_3/ THF-d_8 (8/2, v/v) is less solvated. Although SANS measurements was quite useful for the elucidation of the detailed structure of the PQXs, it was also found that the exhaustive screening of the conditions (temperature, solvents, additives, and so on) were difficult because of the limited neutron beamtime. In this study, we have tried to use small-angle X-ray scattering (SAXS) on a laboratory system.

EXPERIMENTS: A PQX bearing (*R*)-2-octyloxymethyl side chains (100mer) was prepared. The PQX was dissolved in tetrahydrofurane (THF, 4.0 mg / mL) to measure the SAXS patterns by using the Rigaku NANOPIX SAXS/WAXS measurement system (CuKα) or the Rigaku Nano-Viewer X-ray Scattering System (MoKα).

RESULTS: Firstly, we tried to use the Rigaku NANOPIX SAXS/WAXS measurement system (CuKα, λ = 1.54 Å) with an aluminum cell with thin quartz windows (the thickness of the quartz films was 20 μm). However, the adhesive agent (epoxy resin) between the aluminum cell and the quartz films was dissolved in THF, which caused the leak of the liquid sample. Although we have also used the indium seal or other adhesive agents, the leak of the sample was not fully sealed. Subsequently, we tried to use the Rigaku Nano-Viewer X-ray Scattering System (MoKα, λ = 0.71 Å) with a quartz cell with a Teflon cap (the thickness of the quartz windows was 1.0 mm, and the optical path was 2.0 mm), which was used in the SANS measurements. Here, we expected that the wavelength of the X-ray was short enough to measure SAXS patterns using this cell, however, the transmission was found to be not enough. Therefore, we have newly developed a quartz cell with a Teflon cap with thin windows and a short cell path (Fig. 1). The thickness of the quartz windows was shortened to 0.5 mm, and the optical path was also shortened to 1.0 mm. The leak of organic solvents including THF, chloroform, and 1,1,2-tetrachloroethane was not observed at least 24 hours at room temperature. Now we are trying to measure the SAXS pattern of the PQX in various organic solvents using the newly developed quartz cell.

Fig. 1 A quartz cell with a Teflon cap. The thickness of the quartz windows was 0.5 mm, and the optical path was 1.0 mm

REFERENCES:

(1) Yamada, T.; Nagata, Y.; Suginome, M. *Chem. Commun.* **2010**, *46*, 4914-4916.
(2) Nagata, Y.; Yamada, T.; Adachi, T.; Akai, Y.; Yamamoto, T.; Suginome, M. *J. Am. Chem. Soc.* **2013**, *135*, 10104-10113.
(3) Nagata, Y.; Nishikawa, T.; Suginome, M. *J. Am. Chem. Soc.* **2015**, *137*, 4070-4073.
(4) Nagata, Y.; Nishikawa, T.; Suginome, M. *Chem. Commun.* **2012**, *48*, 11193-11195.
(5) Nagata, Y.; Takagi, K.; Suginome, M. *J. Am. Chem. Soc.* **2014**, *136*, 9858-9861.
(6)Nagata, Y.; Uno, M.; Suginome, M. *Angew. Chem. Int. Ed.* **2016**, *55*, , 7126-7130.
(7) Nishikawa, T.; Nagata, Y.; Suginome, M. *ACS Macro Lett.* **2017**, *6*, 431-435.
(8) Nagata, Y.; Nishikawa, T.; Suginome, M.; Sato, S.; Sugiyama, M.; Porcar, L.; Martel, A.; Inoue, R.; Sato, N. *J. Am. Chem. Soc.* **2018**, *140*, 2722-2726.

CO4-13 Vacancy-Type Defects in Tb-Doped GaN Films Probed by a Slow Positron Beam

S. Hasegawa, A. Yabuuchi[1], and A. Kinomura[1]

The Institute of Scientific and Industrial Research, Osaka University
[1]Institute for Integrated Radiation and Nuclear Science, Kyoto University

INTRODUCTION: Rare-earth-doped gallium nitride (GaN) is attracting attention as a candidate material for room temperature ferromagnetic semiconductors. Although the amount of vacancies introduced into the film is considered to be different depending on the crystal growth conditions, they will affect the magnetic properties. In this study, terbium-doped GaN (GaTbN) films were prepared by MBE (molecular beam epitaxy) or ion-implantation techniques, and vacancy-type defects in them were investigated using a slow positron beam.

EXPERIMENTS: Two kinds of MBE-grown GaTbN films with a thickness of around 200 nm were fabricated with different growth conditions. Additionally, a Tb^+-implanted GaN film with a dose of 2×10^{14} Tb^+/cm^2 was also prepared. These films were probed by the KUR slow positron beam and the Doppler broadening of the annihilation radiation (DBAR) spectra were acquired. The DBAR spectra were characterized in terms of an *S*-parameter, which is defined as the peak intensity. When positrons are trapped at vacancy-type defects, the value of *S* increases [1].

RESULTS: Figure 1 shows *S*-parameters obtained for the MBE-grown GaTbN films as a function of incident positron energy. No increase in S-parameters was observed for both GaTbN films compared to the GaN template layer (E > 15 keV). This indicates that Ga vacancies are not introduced by Tb-doping at least under the growth conditions of these samples. Figure 2 shows the annealing temperature dependence of the *S*-parameter obtained for the Tb^+-implanted GaN sample. The increase of the *S*-parameter with increasing the annealing temperature suggests the clustering of the irradiation-induced vacancies. In addition to *S*-parameters corresponding to positron annihilation with low-momentum electrons, *W*-parameters corresponding to annihilation with high-momentum electrons were also determined from the DBAR spectra. The *S*-*W* correlation is shown in Fig. 3. With increasing the annealing temperature, the position of the *S*-*W* plot deviates to the right-hand side from the straight line connecting between the unimplanted-state and the as-implanted-state. This indicates that the irradiation-induced vacancies are clustered by annealing. To observe the interaction between Tb atoms and vacancies, annealing with higher temperatures and comparison with self-ion-irradiated (N^+-implanted) samples are desired.

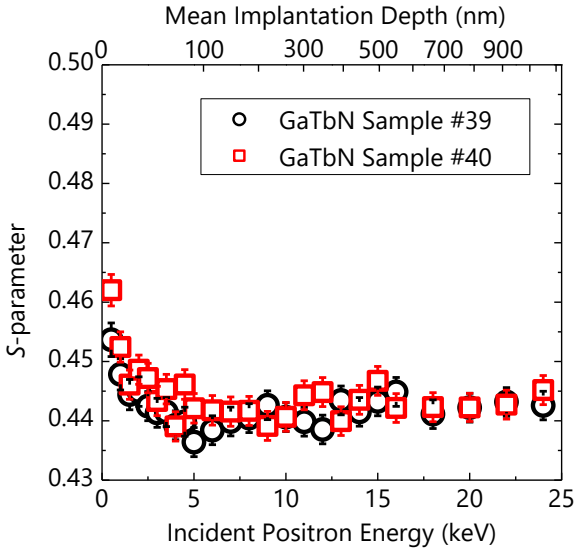

Fig. 1. S-parameters for MBE-grown GaTbN films as a function of incident positron energy. Mean implantation depth is also shown on the upper axis.

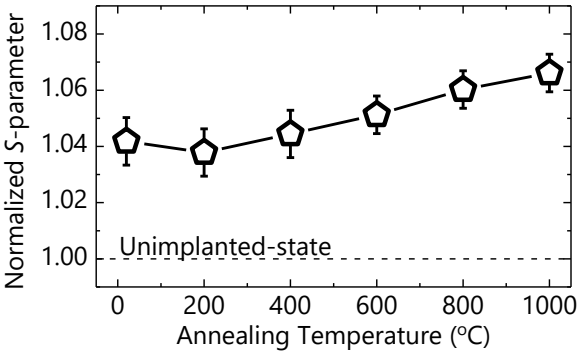

Fig. 2. *S*-parameters for Tb^+-implanted GaN films. The sample was annealed at each temperature for 10 s in N_2 atmosphere by infrared-lamp heating.

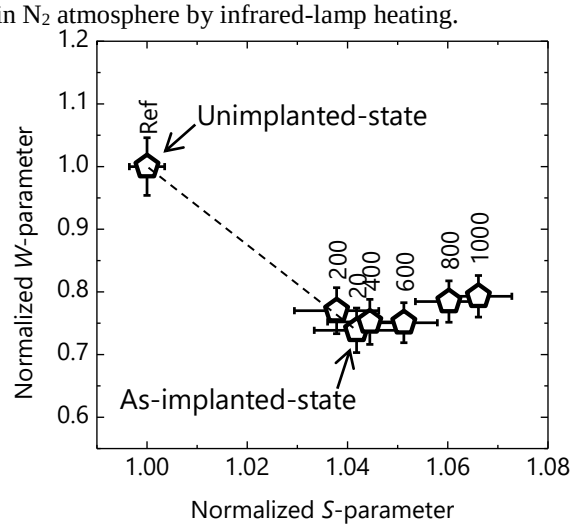

Fig. 3. *S*-*W* correlations for unimplanted (Ref) and Tb^+-implanted GaN films. Annealing temperatures are also shown beside each symbol.

REFERENCES:

[1] R. W. Siegel, Ann. Rev. Mater. Sci., **10** (1980) 393–425.

CO4-14 Fundamental Study on Radiation-Induced Surface Activation under Subcritical Conditions

T. Hazuku[1], T. Ihara[1], R. Taguchi[1], W. Susanto[1], S. Morooka[2], S. Kano[3], H. Abe[3], D. Ito[4] and Y. Saito[4]

[1]*Tokyo University of Marine Science and Technology*
[2]*Waseda University*
[3]*The University of Tokyo*
[4]*KURNS, Kyoto University*

INTRODUCTION: A supercritical water-cooled reactor (SCWR) is one of the 4th generation nuclear reactors, which is based on the light water reactor technology [1], and considered to have high safety and economic performance. On the other hand, radiation-induced surface activation (RISA) phenomenon enhances metal surface wettability, boiling heat transfer and anticorrosive effects by the electrochemical interaction between the base metal and the oxide film on the metal surface [2]. It implies that RISA phenomenon can contribute to the much higher performance of SCWR and improve the safety features.

This study is aimed at evaluations of the RISA effect on the electrochemical characteristics and surface wettability of metals at high-temperatures and pressures.

RESULTS AND DISCUSSIONS:

Effect of RISA on electrochemical characteristics

In order to evaluate the effect of the RISA on the electrochemical characteristics of stainless steels at the subcritical water conditions, corrosion potentials and polarization curves of stainless-304 specimens (SUS-304) before and after radio-activation were measured at the temperatures up to 350 °C. Three types of specimens: the normal SUS-304 with a surface finished by #2000 emery paper, the SUS-304 with SCW oxide film formed in supercritical water with a temperature of 510 °C and pressure around 35 MPa for 90 hours, and the SUS-304 with ZrO_2 spraying film, were used for the electrochemical measurements. The radio-activated specimens were produced by neutron irradiation for 20 minutes at 1 MW in the operation of Kyoto University Research Reactor (KUR). A decrease in corrosion potentials due to radio-activation or the RISA were confirmed for all specimens at temperatures equal to or less than 300 °C (Fig. 1) while the effect of radio-activation on the potentials at a temperature of 350 °C was insignificant for the normal specimen and the specimen with ZrO_2 sprayed film. The decrease in the corrosion potential due to the RISA was, however, more enhanced for the specimen with SCW oxide film even at the temperature of 350 °C. This study first revealed that the electrochemical characteristics of SUS-304 was improved by RISA under the subcritical condition.

Effect of RISA on surface wettability

Next, the capillary action in mini pipes before and after γ-ray irradiation was observed to evaluate the effect of RISA on the metal surface wettability under a subcritical condition. Neutron imaging was used to visualize the water-gas interface in stainless steel capillary pipes. The capillary pipes with various inside diameters such as 0.5, 0.8, 1.2, 1.4, and 1.8 mm were used as a test section which was heated up to a temperature of 320 °C at a pressure of 21 MPa. The pipes irradiated by 60-Co γ-ray with an integrated irradiation dose of approximately 500 kGy and non-irradiated pipes with various diameters are installed in parallel and water levels in each pipe were compared to evaluate capillary action differences (Fig. 2). The measured water level data showed a good agreement with the calculation. The data in the irradiated pipes showed the wettability was decreased compared to non-irradiated pipes at the temperature of 320 °C. Microscopic observation will be required to clarify the relationship between surface wettability and the formation of the hydroxyl groups on the irradiated surface material under high temperatures.

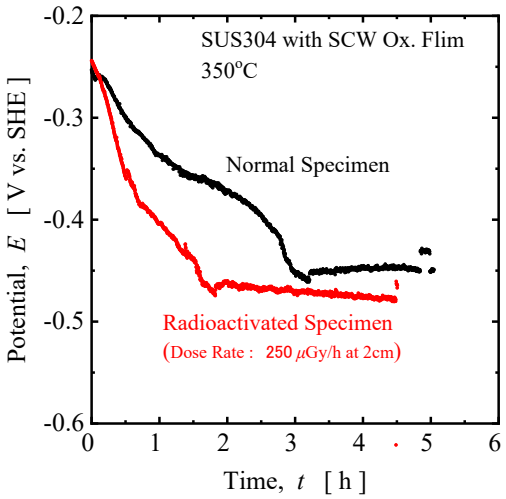

Fig. 1. Corrosion potential of SUS-304 with SCW oxide film before and after radio-activation at 350 °C

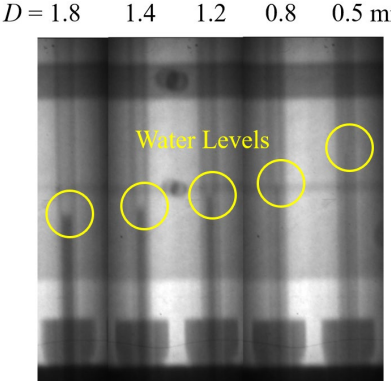

Fig. 2. Typical images in non-irradiated capillary pipes at 320 °C taken by neutron imaging

REFERENCES:

[1] Y. Oka and H. Mori, Supercritical pressure light water cooled reactor, Springer (2014).
[2] T. Takamasa, *et al*., J. AESJ, 49-1 (2007) 45-50.

CO4-15 Salt effects on nanostructure of gliadin hydrates as revealed by SAXS

N. Sato, R. Urade, R. Inoue, K. Morishima, M. Sugiyama

Institute for Integrated Radiation and Nuclear Science, Kyoto University

INTRODUCTION: Wheat flour has been one of the most essential staple foods since ancient times. The quality of wheat flour foods is largely dependent upon the physical property of what dough, which is formed by kneading wheat flour with water and salt. It is well-known that the physical property of wheat dough is mainly attributable to gluten, a composite of major wheat storage proteins: gliadin and glutenin. The former is a monomeric protein responsible for viscosity; the latter is a polymeric protein responsible for elasticity. Therefore deeper understanding on these proteins must be necessary to improve the processability of wheat dough and the quality of wheat food products.

For a long time, gliadins have been believed to be insoluble in water, and accordingly they were extracted with 60–70% ethanol or weak acids. However it has recently been found that gliadins can be extracted into pure water from wheat dough containing NaCl [1]. Seeing that the actual wheat dough is composed of water not alcohols or acids, gliadins in water are more suitable for investigation on the behavior of gliadins in real situation. Based on this view, we have been investigating nanostructure of gliadins in pure water by small-angle X-ray scattering (SAXS). SAXS is a powerful technique for examining structure of disordered condensed materials such as gels, colloids and rubber, and this merit is also effectively applicable to food materials. Our previous study [2] revealed that gliadin monomers dispersed isolatedly at a low concentration of aqueous solution gradually associate together to form multimolecular domains with interdomain interference. The SAXS profiles for gliadin hydrates at higher concentrations also disclosed that density fluctuation exists in the gliadin aggregates and the correlation length of this fluctuation becomes smaller with increasing gliadin concentrations. It was also found that nanostructure of gliadin hydrates is strongly affected by the presence of salts. As the concentration of NaCl increases, the correlation length of density fluctuation reduces significantly, suggesting that gliadin hydrates are strongly contracted. The rheological property of gliadin hydrates also highly depend on the presence of salts. Compression modulus of gliadin hydrates increases with increasing NaCl concentrations. This means that gliadin hydrates become hard when NaCl is added. However it is still unknown what interaction induces the change of structure and property of gliadin hydrates in the presence of salts. In this study, we conducted SAXS measurements on gliadin hydrates containing various classes of salts to elucidate the mechanism of salts affecting on the hydration and association of gliadin molecules.

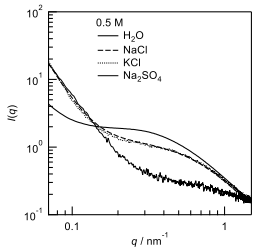

Fig 1. SAXS profiles of 40% gliadin hydrates containing various salts at a concentration of 0.5 M.

EXPERIMENTS: Gliadins prepared by the same method as reported before [1] were dispersed into water containing various kinds of salts at a concentration of 0.5 M. Total gliadin concentration was adjusted by adding the salt-containing solvents whose volume was the same as that of the 40 wt% salt-free solution. Samples were put into 1-nm-thick aluminum cells with optical windows of 7-μm-thick PEI films. SAXS measurements were performed with a laboratory SAXS instrument (NANO-PIX, Rigaku) installed at Institute for Integrated Radiation and Nuclear Science, Kyoto University. The wavelength of X-ray was 1.54 Å and the camera length was 1300 mm. Typical exposure time was 300 sec. All measurements were carried out at 25 °C.

RESULTS: Fig. 1 shows the results of SAXS measurements with 40 wt% gliadin solutions with 0.5M NaCl, KCl and Na_2SO_4. A broad peak due to density fluctuation was found at q = 0.4 nm^{-1} in pure water, and it became small and shifted higher to q = 0.4 nm^{-1} by adding 0.5M NaCl. This profile was almost unchanged by altering salt with KCl, implying that cation variation has little effect on the nanostructure of gliadin hydrates. In contrast, the profile for Na_2SO_4 was drastically different. The broad peak due to density fluctuation was hardly recognizable. This fact indicates that anion change has more significant influence on aggregation structure of gliadin hydrates. Also it should be noted that valence number of the anion is larger than chloride ion, which affects the electrostatic interaction between the gliadin molecules.

REFERENCES:

[1] T. Ukai, Y. Matsumura, R. Urade, *J. Agric. Food Chem.*, **56**, (2008) 1122-1130.

[2] N. Sato, *et al., J. Agric. Food Chem.*, **63**, (2015) 8715-8721.

CO4-16 Ar$^+$-Irradiation-Induced Defects in $GdB_2Cu_3O_y$ Superconducting Films Probed by Positrons

T. Ozaki, T. Sueyoshi[1], H. Sakane[2], A. Yabuuchi[3] and A. Kinomura[3]

School of Science and Technology, Kwansei Gakuin University
[1]Faculty of Advanced Science and Technology, Kumamoto University
[2]SHI-ATEX Co., Ltd.
[3]Institute for Integrated Radiation and Nuclear Science, Kyoto University

INTRODUCTION: $GdBa_2Cu_3O_y$ (GdBCO) is attracting attention as a candidate material for superconducting wires that can be used in liquid nitrogen temperatures. Recently, it has been found that ion-irradiation-induced defects allow the magnetic flux to be pinned and remain superconducting-state even under high magnetic fields. However, it has not been clarified what defects formed by ion irradiation are effective as pinning points. In this study, to investigate what kind of defect that improves high magnetic field resistance in superconducting materials, Ar$^+$ ions irradiated GdBCO samples were probed by a slow positron beam.

EXPERIMENTS: 350 keV Ar$^+$ ions were irradiated to GdBCO(500 nm)/CeO_2(150 nm)/Y_2O_3(150 nm)/Ni/Cu/SUS samples with doses of 5.6×10^{12} Ar$^+$/cm^2 or 3.5×10^{13} Ar$^+$/cm^2. In this Ar$^+$ beam energy, irradiation-induced defects are formed only in the GdBCO layer with a thickness of 500 nm. The unirradiated and Ar$^+$ irradiated GdBCO samples were probed by the KUR slow positron beam and the Doppler broadening of the annihilation radiation (DBAR) spectra were acquired. The DBAR spectra were characterized by *S*-parameter (*W*-parameter), which corresponding to annihilation with low (high) momentum electrons [1]. When positrons are trapped at vacancy-type defects, the value of *S* increases [1].

RESULTS: Figure 1 shows the *S*-parameters obtained for each sample. Contrary to our initial expectations, decreases in S-parameters are observed after Ar$^+$ irradiation. Since the value of S does not increase even when the irradiation dose becomes 6 times or more, almost all incident positrons are considered to be trapped at irradiation-induced defects. Figure 2 shows *S*-*W* correlations obtained for each sample acquired at incident positron energies of 6–11 keV. In the two irradiated samples, the *S*-*W* correlations are plotted in approximately the same region. Almost all positrons are trapped at defects in the irradiated samples, thus, this result indicates that positrons are trapped at the same defect species in both samples. On the other hand, the *S*-*W* correlations of the unirradiated sample are plotted in the region where *S* is higher than that of the irradiated samples. This means that the unirradiated sample contains larger vacancy-type defects (vacancy clusters or voids) than in the irradiated samples. The observed decreases in S parameters due to Ar irradiation will be caused by the mechanism as shown in Fig. 3. Briefly, the unirradiated sample contains larger as-grown defects than Ar$^+$-irradiation-induced defects.

REFERENCE:

[1] R. W. Siegel, Ann. Rev. Mater. Sci., **10** (1980) 393–425.

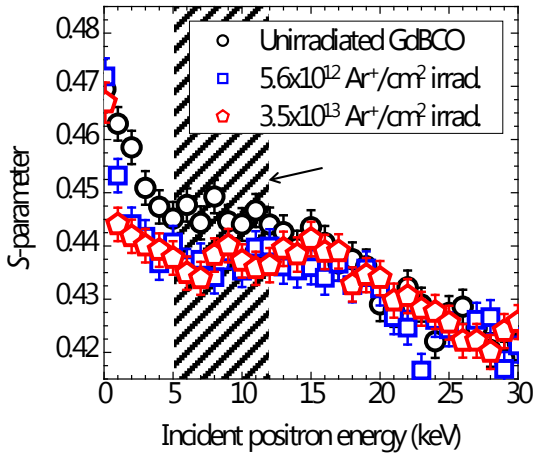

Fig. 1. *S*-parameters for unirradiated and Ar$^+$ irradiated GdBCO samples.

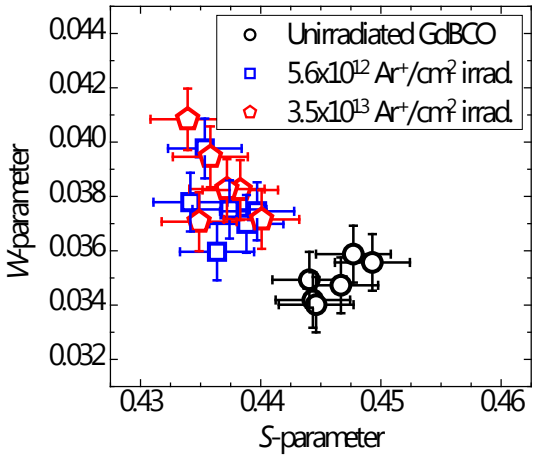

Fig. 2. *S*-*W* correlations for unirradiated and Ar+ irradiated GdBCO samples acquired at incident positron energies of 6–11 keV.

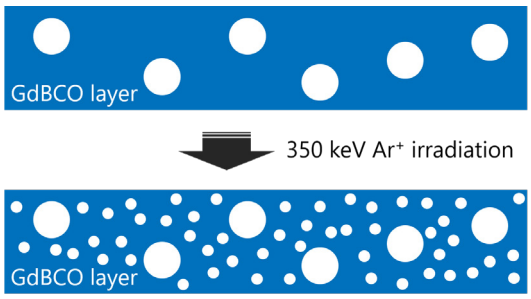

Fig. 3. Picture explaining the change of positron annihilation characteristics in the GdBCO layers before and after Ar$^+$ irradiation.

CO4-17 Vacancy migration behavior in Co-Cr-Fe-Mn-Ni medium/high entropy alloys

K. Sugita, M. Mizuno, H. Araki, A. Yabuuchi[1] and A. Kinomura[1]
Graduate School of Engineering, Osaka University
[1]*Institute for Integrated Radiation and Nuclear Science, Kyoto University*

INTRODUCTION: The alloy design has been conventionally performed by choosing a base metal and adding suitable elements to achieve desired properties. Over the last decade, a new type of multicomponent alloys called as "high entropy alloys", which include equiatomic / near-equiatomic proportion of constituent elements, have been proposed by Yeh et al. [1-3]. They often show simple solid solution structures at high temperature due to high configurational entropy of mixing for a random solid solution. High entropy alloys have been reported to have the following promising properties of practical interest, such as high strength combined with ductility, high fracture toughness, excellent oxidation and corrosion resistance. "Sluggish diffusion" kinetics is believed to be a main contributor to these properties. Therefore, it has also created fundamental interest for atomic diffusion in a multiprincipal element matrix, and the diffusion kinetics in high entropy alloys has been actively investigated by diffusion couple method and tracer-diffusion method.
In this work, we contribute to a debate about hypothetical sluggish diffusion phenomena in high entropy alloys by investigating the vacancy migration behavior in Co-Cr-Fe-Mn-Ni medium/high entropy alloys during the isochronal annealing after electron-irradiation.

EXPERIMENTS: Metal pieces of Co, Cr, Fe, Mn and Ni with 99.9% up purity were added together in equiatomic proportions to produce $Co_{20}Cr_{20}Fe_{20}Mn_{20}Ni_{20}$, $Co_{25}Fe_{25}Mn_{25}Ni_{25}$, $Co_{25}Cr_{25}Fe_{25}Ni_{25}$, $Cr_{33.4}Fe_{33.3}Ni_{33.3}$, $Cr_{15}Fe_{45}Ni_{40}$ alloy ingots by arc melting or vacuum induction melting followed by homogenization at 1373 K for 24 h. The alloy ingots were cut into square plate specimens with dimensions of 10 × 10 × 0.5 mm^3. The specimens were subjected to strain relief annealing at 1373K for 10 h and then rapidly cooled to prevent secondary phase precipitation and to stabilize single-phase FCC structures. The specimens in water flow were exposed to 8 MeV electron beam irradiation for 3 h in KURNS-LINAC. The irradiation damage was evaluated at (1.3 - 1.8) $\times 10^{-4}$ dpa. In order to investigate the thermal stability of vacancies, the electron irradiated specimens were subjected to the subsequent isochronal annealing for 1 h at 373-673 K.
Positron lifetime measurements were carried out by using a digital oscilloscope system with photomultiplier tubes mounted with BaF_2 scintillators, having a time resolution (FWHM) of 180 ps. The positron lifetime measurements require data acquisition for approximately 15 hours with a Na-22 positron source of 0.5 MBq activity in order to acquire 3 million counts in the positron lifetime spectrum. The measured spectra were analyzed using the programs RESOLUTION and POSITRONFIT Extended.

RESULTS: Mean positron lifetime in the electron-irradiated specimens after isochronal annealing is shown in Fig.1. The positron lifetime spectra of as-irradiated specimens show a clear splitting into two exponential components with the longer lifetime values of 185-195 ps. This indicates that a part of positrons is trapped by monovacancies and relatively small vacancy clusters produced during the electron beam irradiation. After the subsequent isochronal annealing, the mean positron lifetime is observed to decrease sharply around 473K. This can be attributed to the decrease in vacancy concentrations triggered by the free vacancy-migration. It demonstrates the vacancy migration enthalpy in the CoCrFeMnNi high entropy alloy is very similar to that in the CrFeNi alloy. These results indicate that the "'sluggish diffusion" hypothesis is not supported in Co-Cr-Fe-Mn-Ni medium/high entropy alloys at least in view of vacancy migration behavior.

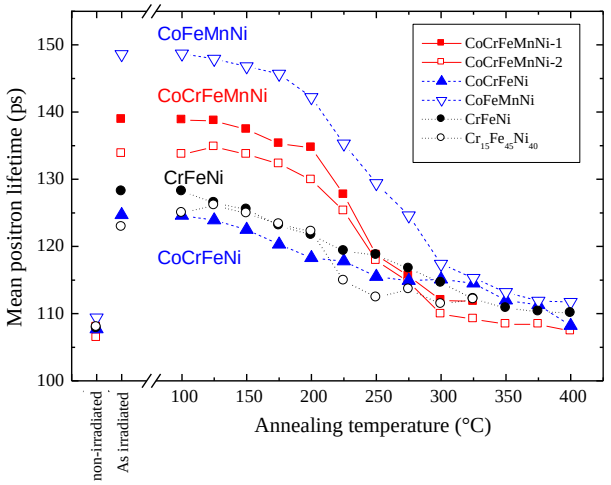

Fig. 1 Mean positron lifetime in the electron-irradiated CoCrFeMnNi, CoFeMnNi, CoCrFeNi, CrFeNi alloys after isochronal annealing.

REFERENCES:
[1] C. Y. Hsu, J. W. Yeh, S. K. Chen, T. T. Shun: Metall. Mater. Trans. 35A, (2004), 1465.
[2] J. W. Yeh, S. K. Chen, S. J. Lin, J. Y. Gan, T. S. Chin, T. T. Shun, C. H. Tsau, S. Y. Chang: Adv. Eng. Mater. 6 (2004). 299.
[3] J. W. Yeh: Ann. Chim. Sci. Mat. 31, (2006), 633.

CO4-18 **Recovery Behaviors of Irradiation-Induced Vacancies in Tungsten Probed by Positrons**

A. Yabuuchi, M. Tanaka and A. Kinomura

Institute for Integrated Radiation and Nuclear Science, Kyoto University

INTRODUCTION: Generally, excess-introduced vacancies agglomerate in the annealing process and develop into vacancy clusters. However, in recent years, vacancies in tungsten (W) have been predicted to repulse each other in theoretical studies based on the first principle calculations [1,2]. In this study, recovery behaviors of electron-irradiation-induced vacancies in W were investigated using positron annihilation lifetime spectroscopy.

EXPERIMENTS: W plates ($5\times10\times0.8$ mm^3) with a purity of 99.999% (5N) were annealed at over 2273 K in vacuum to eliminate lattice defects. After the annealing, 8 MeV electrons were irradiated to the samples at around 373 K using the KURNS-LINAC with total doses of 5×10^{19} e$^-$/cm^2 or 1×10^{18} e$^-$/cm^2. The irradiated samples were isochronally annealed in steps of 15 min/50 K in a vacuum. Positron annihilation lifetime measurements were performed at room temperature for each annealing temperature.

RESULTS: Figure 1 shows the change in positron lifetimes obtained for the 5×10^{19} e$^-$/cm^2 irradiated sample during the isochronal annealing. A positron lifetime component corresponding to a monovacancy [3] is observed in the as-irradiated state with a relative intensity of about 90%. The longer positron lifetime component τ_2 clearly increases at about 600 K. This indicates that monovacancies in W aggregate to form vacancy clusters. Such vacancy clusters are substantially eliminated after the 1423 K annealing. On the other hand, it is noticed that the observed τ_1 is longer than τ_1^{TM} estimated from τ_2 and I_2 with assuming only one defect species exists in the sample. This means that positrons are also trapped at other defect species having a shorter positron lifetime than monovacancies. Figure 2 also shows the change in positron lifetimes obtained for the 1×10^{18} e$^-$/cm^2 irradiated sample during the isochronal annealing. In this measurement, the observed τ_1 agrees with the calculated τ_1^{TM}, which indicates that positrons not trapped at the defect corresponding to the longer positron lifetime τ_2 are annihilated in the delocalized state. However, the longer lifetime component is shorter than that of the high dose sample mentioned above and is less than 150 ps. These results suggest that interstitial impurities are bound with vacancies. Our recent theoretical calculation also supports the interpretation.

REFERENCE:

[1] L. Ventelon *et al.*, J. Nucl. Mater., **425** (2012) 16-21.
[2] Y. Oda *et al.*, Plasma Fusion Res., **9** (2014). 3401117-1-3401117-4.
[3] K. Sato *et al.*, Nucl. Mater. Energy, **9** (2016) 554-559.

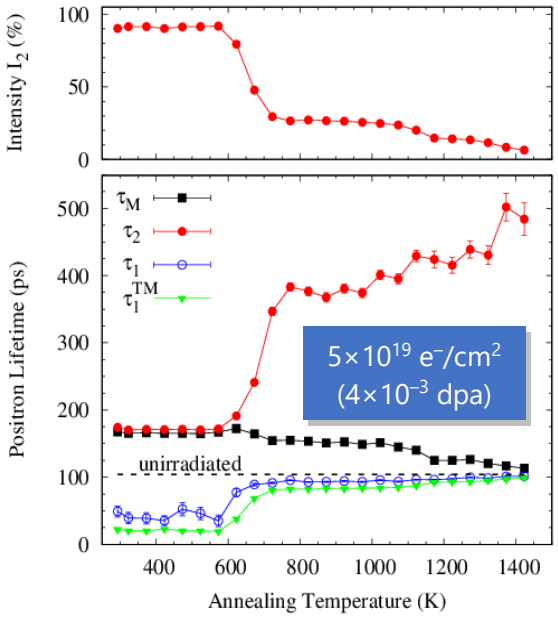

Fig. 1. Change in mean positron lifetime (τ_M), resolved lifetimes (τ_1, τ_2), and the relative intensity of the longer lifetime component (I_2) on isochronal annealing (15 min/50 K) of 5N-W irradiated around 373 K with 8 MeV electrons to a total dose of 5×10^{19} e$^-$/cm^2. The τ_1 calculated from τ_2 and I_2 assuming the presence of only one defect species is shown as τ_1^{TM}. Unirradiated-state is indicated by a horizontal dashed line.

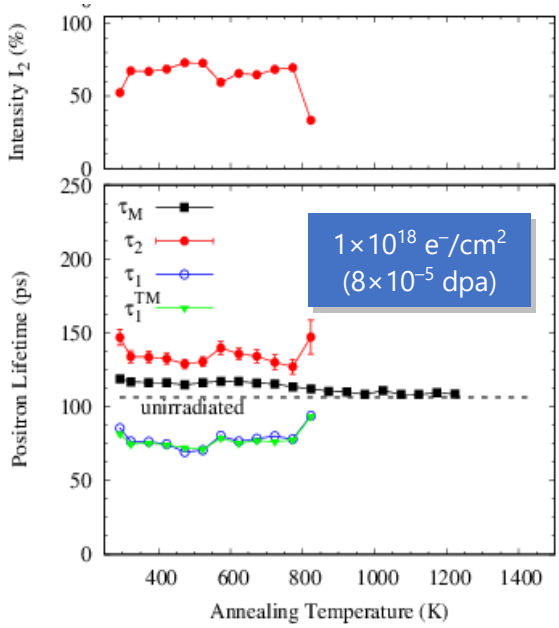

Fig. 2. Change in mean positron lifetime (τ_M), resolved lifetimes (τ_1, τ_2), and the relative intensity of the longer lifetime component (I_2) on isochronal annealing (15 min/50 K) of 5N-W irradiated around 373 K with 8 MeV electrons to a total dose of 1×10^{18} e$^-$/cm^2. The τ_1 calculated from τ_2 and I_2 assuming the presence of only one defect species is shown as τ_1^{TM}. Unirradiated-state is indicated by a horizontal dashed line.

CO4-19 Spectrum of Amino Acid in the Sub-THz region using Coherent TR (II)

T. Takahashi

Institute for Integrated Radiation and Nuclear Science, Kyoto University

INTRODUCTION: In recent years various types of coherent radiation emitted from a short bunch of relativistic electrons have attracted a considerable attention as a bright light source in the THz-wave and millimeter wave regions for the spectroscopic purpose. Coherent transition radiation (CTR), which is emitted from a boundary between two media, is one of such a coherent light source. CTR is usually utilized as a non-polarized light source, because the electric vector of transition radiation (TR) emitted from a metallic screen is axially symmetric with respect to the trajectory of an electron beam. In my previous reports [1] the circularly polarized CTR using a pair of wire-grid radiators with the different polarization has been developed with a new idea. Circularly polarized light has been useful in the circular dichroism spectroscopy. In my previous reports [2] spectra of some kinds of chiral amino acid have been measured using linearly polarized CTR. In this report spectra of Adenine and Thymine, which construct DNA, have been measured.

EXPERIMENTAL PROCEDURES: The experiment was performed at the coherent radiation beamline [3] at the L-band linac of the Institute for Integrated Radiation and Nuclear Science, Kyoto University. The energy, the width of the macro pulse, and the repetition rate of the electron beam were 42 MeV, 47 ns, and 60 Hz, respectively. The average current of the electron beam was 2.0 μA. The spectrum of CTR was measured by a Martin-Puplett type inter- ferometer and a liquid-helium-cooled Si bolometer. The schematic diagram of the experiment was shown in Fig.1.

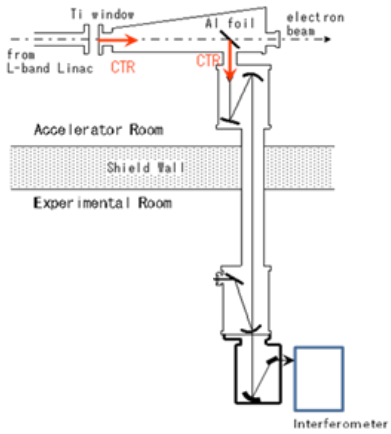

Fig.1 The schematic diagram of the experiment.

Figure 2 is the photograph of the spectrometer and the detector.

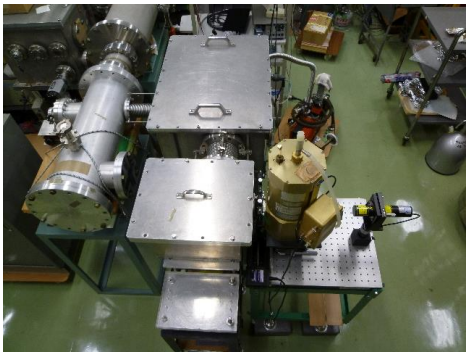

Fig.2 The photograph around the spectrometer.

RESULTS: Measured spectra of Adenine and Thymine are shown in Figs. 3. In the spectrum of Thymine some absorptions are observed at 15, 14, and 19 cm^{-1}. The identification of observed absorption is now in progress

REFERENCES:

[1] T. Takahashi, *et al.*, KURRI-PR 2015 CO4-7.
[2] T. Takahashi, *et al.*, KURRI-PR 2016 CO4-8.
[3] T. Takahashi *et al.*, Rev. Sci. Instrum. **69** (1998) 3770.

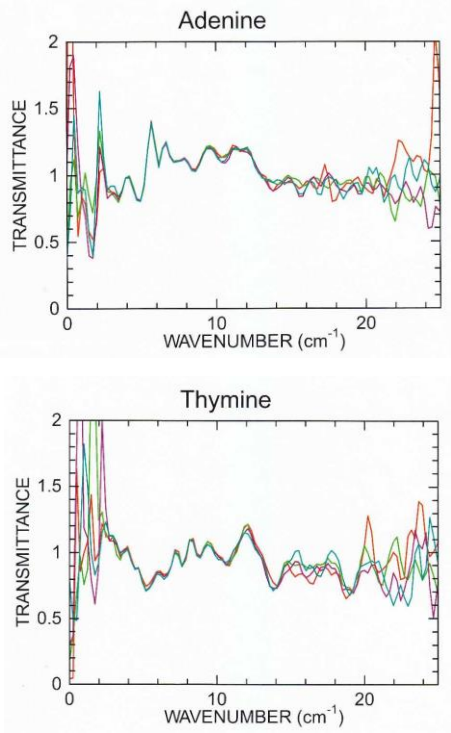

Fig.3 Spectra of Adenine and Thymine.

30080

CO4-20

Hydrogen retention on plasma facing material irradiated by high energy particle beam

K. Tokunaga, M. Matsuyama[1], M. Hasegawa, K. Nakamura and Q. Xu[2]

Research Institute for Applied Mechanics, Khushu University
[1]Hydrogen Isotope Research Center, University of Toyama
[2]Institute for Integrated Radiation and Nuclear Science, Kyoto University

INTRODUCTION: It is of importance to clarify phenomena of implantation, retention, diffusion and permeation of tritium on surface of the armor materials of the first wall/blanket and the divertor on fusion device from a viewpoint of precise control of fuel particles, reduction of tritium inventory and safe waste management of materials contaminated with tritium (T). Refractory metals such as tungsten (W) is potential candidate for an armor of the first wall and the divertor plate of the fusion reactor because of its low erosion yield and good thermal properties. The armor material will be subjected to heavy thermal loads in the steady state or transient mode combined with high energy neutron irradiation that will cause serious material degradation. In addition, high energy runaway electrons would bombard the armor materials along the equatorial plane in fusion device. It is considered that these cause radiation damage and enhance tritium retention. In the present works, T exposure experiments have been carried out on W samples which were irradiated by high energy electrons using LINAC in KURRI of Research Reactor Institute, Kyoto University to investigate effects of high energy electrons irradiation and microstructure on tritium retention of W. In this fiscal year, pure W and recrystallized W were irradiated by high energy electron beam. After that, positron annihilation experiment was carried out to identify the radiation defect. In addition, tritium exposure experiments have been carried out using a tritium (T) exposure device.

EXPERIMENTS: W samples used were ITER grade W (IG-W) and recrystallized W. In the case of IG-W, one was W sample (ITER grade W(1)) which the surface were manufactured to be oriented parallel to the rolling surface and rolling direction. The other W sample (ITER grade W(3)) which the surface were manufactured to be oriented perpendicular to the rolling surface and rolling direction. On the other hand, heat treatment was performed at 1800 ºC for 1h at high vacuum to recrystallize IG-W. The sizes of W samples were 10mm x 10mm x 1mm. The surface of the both samples were polished to be mirrored. High energy electrons irradiation has been carried out using LINAC in KURRI of Research Reactor Institute, Kyoto University. An energy of electron irradiated was 10 MeV and DPA was 2.8 x 10^{-3}. Temperature during the irradiation was measured by thermocouples which was contacted with a backside of the W samples. After the electron beam irradiation, positron annihilation experiment was carried out. In addition, T exposure experiments have been carried out using a T exposure device in University of Toyama. Pressure of the T gas was 1.3 kPa and T exposure was kept for 4 h. T concentration in the gas was about 5 %. Temperatures of pre-heating and T exposures were 400 ºC and 350 ºC. After the exposure to T gas, T amount retained in surface layers of the sample was evaluated by β-ray-induced X-ray spectrometry (BIXS) and imaging plate (IP) measurements.

RESULTS: In the condition of 10 MeV electrons irradiation, electrons go through in 1 mm thickness W sample. As a result, uniform defects were formed in the W samples. Figure 1 shows amount of T measured by the IP measurement. Large amount of T traps comparing with that of samples exposured at 100 ºC, which was reported in the last fiscal year. In the case of non-irradiated samples, T retention of non-recrystallized samples is larger than that of recrystallized samples. These results indicated that some kinds of defects which can trap T decreased by the recrystallization. After the electron beam irradiation, amount of T of non-recrystallized samples is almost the same of that of the un-irradiated ones. However, in the case of the recrystallized samples, the amounts of T of electron beam irradiated samples are a few times of that of non-irradiated samples. As at 400 ºC, vacancies which were produced by electron irradiation at RT, can move enough, vacancy clusters were also formed. It is considered that these vacancy clusters also trap T.

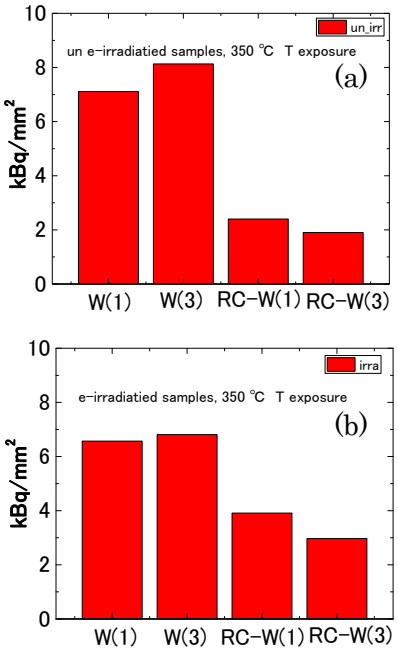

Fig. 1. Amount of tritium on before(a) and after(b) electron beam irradiation measured by IP measurement. RC-W(1) and RC-W(3) are recrystallized W(1) and W(3), respectively.

CO4-21 Defects structure and characterization of electron irradiated B2 ordered alloys

F. Hori, K. Sugita, Y. Sumikura, A. Takano, K. Ohsawa[1], Q. Xu[2] and N. Abe[2]

Dept. of Quantum & Radiation Eng., Osaka Pref. Univ.
[1]*Res. Inst. of Appl. Mech., Kyushu University*
[2]*KURNS, Kyoto University*

INTRODUCTION: Fe-Al alloys, which is B2 ordered intermetallic compound, have good properties such as specific strength to weight ratio, oxidation resistance and strength in elevated temperature. However, the nature of basic defects in this alloy is not necessarily cleared yet. Namely, intermetallic compound alloys possibly include more than two types of vacancies, basically A-vacancy and B-vacancy in A-B type compound. It is difficult to distinguish these vacancies and their characteristic features are distinguishable. For instance, different interaction of hydrogen atoms and different type of vacancies in B2 ordered Fe-Al alloy is suggested by the first principle calculation. So far, we have successfully produced Rh-vacancy and Fe-vacancy by different energy of electron irradiation in Fe-Rh alloys and also detected these defects by positron annihilation techniques. On the other hand, hydrogen is nowadays receiving a lot of attention for various kinds of materials research. It is important to clear the interaction between hydrogen and metallic materials for example hydrogen embrittlement, hydride formation and hydrogen induced transformation in hydrogen storage material. In this study, we have studied the interaction between hydrogen atom and non-equilibrium vacancies in B2 ordered intermetallic alloys.

EXPERIMENTS: Fe-50%Rh alloy specimens with B2 ordered structure were prepared by arc melting method. Sliced samples with the thickness of 0.5 mm were annealed at 1073 K for 3 h followed by quenched into water. These specimens were irradiated with 2 MeV electron to the fluence of 1×10^{17} and 1×10^{18} /cm^2 at JAEA-Takasaki and with 8 MeV electron to the fluence of 5×10^{17} and 1×10^{18} /cm^2 at KURRI, Kyoto University. In both cases, irradiations were carried out at about 330 K controlled by water flow system. Cathodic charged hydrogen implantation have performed for before and after irradiated samples. All samples were measured by X-ray diffraction, positron annihilation lifetime and coincidence Doppler broadening measurements. Also thermal desorption spectroscopy (TDS) measurement have done for hydrogen implanted alloy samples with annealing up to 800K.

RESULTS: Figure 1 shows the CDB ratio profiles of Fe-Rh alloys before and after electron irradiation and hydrogen charged alloy with irradiation. Positron lifetime and CDB results reveals that this irradiation mainly introduces V_{Fe} in this alloy. Changing profile of CDB after hydrogen charging showing trapping of hydrogen atoms by the vacancies. Figure 2 shows the hydrogen desorption from cathodic charged Fe-Rh alloy with or without irradiation. In this figure, desorption peak at 770K appears for hydrogen charged with irradiation sample. Then it can be concluded that hydrogen atoms are trapped by vacancies and released them at this temperature.

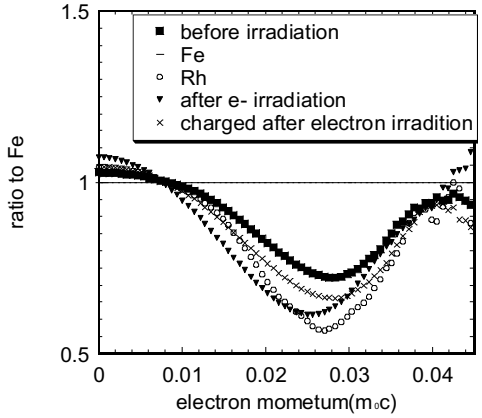

Fig. 1 CDB ratio spectra of electron irradiated and cathodic charged samples.

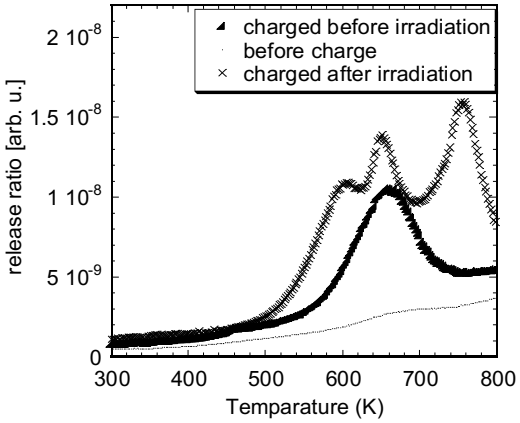

Fig. 2 TDS spectrum for all samples. Hydrogen desorption behavior with annealing temperature.

CO4-22 **Synthesis of Pd nanoparticles on various support materials by γ-ray irradiation reduction method**

F. Hori, S. Toda, Y. Uchimura, T. Matsui[1], Y. Mizukoshi[2] and Q.Xu[3]

Dept. of Engineering, Osaka Prefecture University
[1] Center for Advanced Education of Entrepreneurship and Innovation, Osaka Prefecture University
[2]Institute of Materials Research, Tohoku University
[3]KURNS, Kyoto University

INTRODUCTION: It is well known that metal nanoparticles (NPs) have some specific properties, which are not appeared in bulk materials such as catalytic activities, magnetic properties, electric conductivity and light absorption. These properties depend on its size, shape, structure, chemical composition and so on. They have many possibilities to applied for various industrial fields. Generally, many kinds of metal NPs commercially are synthesized by using chemical reaction method, which is not necessarily in water solution. We have been trying to synthesize various kinds of metal nanoparticles with size and shape controlled by gamma-ray irradiation reduction method. Generally, NPs are not only used itself but supported on large particles with the order of micrometer in almost case. So far, nanocomposites composed of graphene support material and noble metal NPs were successfully synthesized in one-pot process by gamma-ray irradiation. In this study, we have tried to control the size distribution of noble metal NPs on support materials by adsorbing the metal ions on the surface of support material before gamma-ray irradiation.

EXPERIMENTS:
Aqueous solutions with a given concentration of Pd(II) ($PdCl_2 \cdot 2NaCl \cdot 3H_2O$) and 2-propanol. Al_2O_3 and PMMA (Polymethyl methacrylate) powders were added into each water solution respectively. The solution was argon gas purged and sealed into polystyrene vessels. After dispersion by an ultrasonic cleaning bath, they were irradiated with γ-rays from ^{60}Co radio active source at gamma irradiation facility in KURRI, Kyoto University. In order to compare the adsorbing effect of Pd ions on the support materials, one sample was irradiated just after ultrasonic irradiation and another one was gamma irradiated after leave standing for 96 hours. The total dose of gamma irradiation was fixed to 10 kGy with dose rate of 13.6 kGy/h. After irradiation, the products were separated by centrifugation, washed with water and dried by freeze-drying. UV–vis absorption spectra were measured and all products were observed by conventional TEM (JEM-2000FX). X-ray Photoelectron Spectroscopy (XPS) measurement at KEK-PF BL-27 has performed.

RESULTS:
Fig. 1 shows the TEM images for Pd NPs formed on Al_2O_3 particles in aqueous solutions by gamma-ray irradiation reduction. Fig. 2 shows the TEM images for Pd NPs formed on PMMA in aqueous solutions by gamma-ray irradiation reduction. X ray diffraction and XPS measurements show that all of these particles are pure Pd with fcc structure. In both figures, it found that the size of NPs on the support materials irradiated after leave standing for 96 hours becomes smaller than 10 nm and their size distribution is mono-dispersive compared with no leave standing treated samples. In our previous work and preliminaly experiments, no size change was observed for same experiments of Pd NPs synthesis with graphene support material [1, 2]. Al_2O_3 and PMMA have a fuctional group on their surface but graphene has not. Then, it is considred that the metal ions are adsorped on the surface of support materials and it becomes the nucleation site of NPs growth during reduction by gamma irradiation.

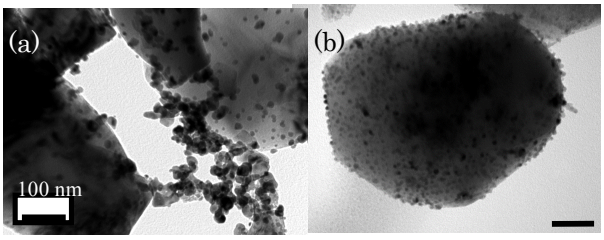

Fig.1 TEM images of Pd NPs reduced with Al_2O_3 by gamma-irradiation method, (a) irradiated just after stirring and (b) irradiated after leave standing for 96 hours.

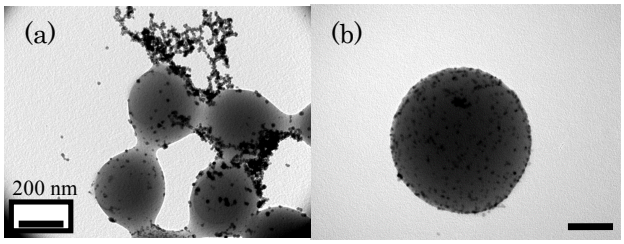

Fig. 2 TEM images of Pd NPs reduced with PMMA by gamma-irradiation method, (a) irradiated just after stirring and (b) irradiated after leave standing for 96 hours.

Reference
[1] A.Tokai and F.Hori et al, Rad. Phys. Chem. 123 (2016) 68.
[2] F.Hori, *et.al,* KURRI Progress Report 2016 (2017) 71 .

CO4-23

Free volume in γ-rays-irradiated Fused Quartz by Positron Age-MOmentum Correlation (AMOC) measurements

H. Tsuchida[1,2], S. Konishi[1], Q. Xu[3]

[1]*Department of Nuclear Engineering, Kyoto University*
[2]*Quantum Science and Engineering Center, Kyoto University*
[3]*Institute for Integrated Radiation and Nuclear Science, Kyoto University*

INTRODUCTION: We study the effect of radiation dose on properties of a free volume in fused quartz under γ-rays irradiation. Fused quartz is a candidate material for use under a radiation environment. A systematic investigation concerning the change in its optical properties has been reported for various types of ionizing radiation such as photons (UV lights and γ-rays), neutrons [1], and fast ions [2]. In this work, Positron Age-MOmentum Correlation (AMOC) technique was applied for investigating radiation damage in the vicinity of free volume by high dose γ-rays irradiation. The AMOC measurement combines positron lifetime and annihilation γ-ray Doppler-broadening spectroscopy by correlated measurements of the positron age and the Doppler shift of one of the annihilation quanta.

EXPERIMENTS: The irradiation experiments were performed at Co-60 γ-rays irradiation facility at KURNS. Fused quartz, with purity of 99.9%, mass density of 2.2 g/cm^3 and thickness of 2 mm (Goodfellow Co.), was used as a target sample. The sample was irradiated with γ-rays at two different radiation doses of 30 kGy and 300 kGy at room temperature. The dose rate was 10 kGy/h. Position annihilation analysis was performed by our developed AMOC system combined with $\beta^+-\gamma$ coincidence positron lifetime spectroscopy. The positron source used was Ge-68.

RESULTS: Fig. 1 shows comparison of positron lifetime spectra obtained before and after irradiation. The spectra in upper left and right indicate results observed at radiation doses of 30 kGy and 300 kGy, respectively. There is a difference in long-lived lifetime component in the time range above approximately 1 ns. This component is attributed to the pick-off annihilation of ortho-positronium (o-Ps) in a free volume of fused quartz. Its intensity is significantly decreased in the spectrum observed after irradiation.

To obtain information about positron lifetimes and corresponding intensities of the spectra, we performed spectrum analysis using the PALSfit program [3]. The results are listed in Table 1. The lifetime and intensity remain unchanged up to 30 kGy, while those values were significantly decreased at high radiation dose of 300 kGy. This suggests that the o-Ps formation in a free volume is suppressed owing to the radiation-induced damage.

The *S* parameter was significantly decreased at 30 kGy, and then it becomes constant. This implies that γ-rays irradiation does not affect a change in a density of free volume in fused quartz. We will perform further investigation on processes of o-Ps annihilation depending on radiation dose by AMOC measurements.

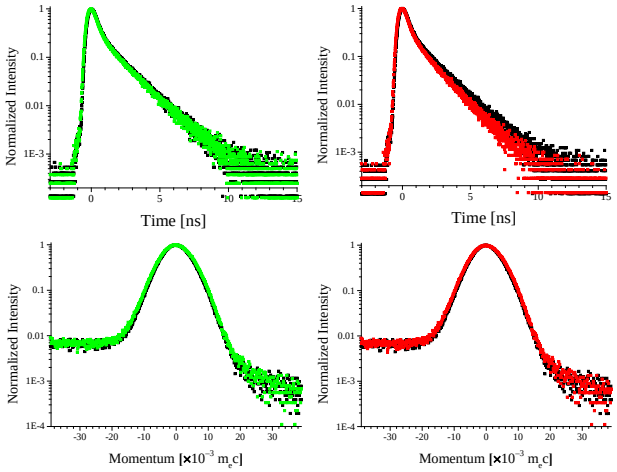

Fig. 1. Spectra of positron lifetime (upper) and annihilation γ-ray Doppler-broadening (bottom) obtained from AMOC measurements for fused quartz sample obtained before and after irradiation of Co-60 γ-rays. The data in left and right shows results for radiation doses of 30 kGy and 300 kGy, respectively. Black symbol indicates data observed before irradiation.

Table 1. Radiation does dependence of the o-Ps lifetime (τ) and intensity (*I*), and the line-shape parameter *S*. The results were obtained from analysis of data shown in Fig. 1.

Dose (kGy)	τ (ns)	*I* (%)	*S*
0	1.580 ± 0.005	53.0 ± 0.2	0.535 ± 0.001
30	1.591 ± 0.005	50.0 ± 0.2	0.509 ± 0.001
300	1.455 ± 0.005	47.8 ± 0.2	0.512 ± 0.001

REFERENCES:

[1] C.D. Marshall *et al.,* J. Non-Crystal. Solids, **212** (1997) 59.
[2] H. Tsuchida *et al.*, Mater. Res. Express, **3** (2016) 055201.
[3] *PALS-Fit Computer Program* (http://palsfit.dk/).

CO4-24 Complex Structure of Ions Coordinated with Hydrophilic Polymer 19. Application for Metaric Plating on Resin Surface. (3)

A. Kawaguchi and Y. Morimoto

KURNS, Kyoto University

INTRODUCTION:

We have reported interacted structures between iodine (polyiodide ions, I_n^{m-}, *m*, *n*: integer, $n > 1$) and polymers.[1] While polyiodide ions (and their counter-ions, ex. K^+ ion presented within I_2-KI(aq)) are prepared as solutes in aqueous solution, they can be diffused into various polymeric matrix without softening nor melting. Such structures and procedures are expected to introduce novel functionality and wide applications to modify polymeric materials with easy operation.[2]

Or, ionic diffusion of polyiodide ions and their counter ions from aqueous solution of polyiodides ("(1st) iodine doping") can advance not only into hydrophilic polymers, such as polyamide-6 (PA6) or polyvinyl-alcohol (PVA), but also into hydrophobic polymers, such as polyethylene (PE) or polyethylene-terephthalate (PET); polyiodide ions in the aqueous solutions can easily diffuse even into *hydrophobic* matrices at room temperature. without melting.

Furthermore, posterior ionic diffusion on the previous presence of polyiodides ("secondary doping") can also advances for both hydrophilic polymers and hydrophobic ones. As phenomena, (previously) iodine-doped polymers can be regarded as "pseudo solvents" for ionic diffusion.[3,4]

These results suggest that coordination between iodine and polymers is dynamic and pliable and activated process, and that previous existence of polyiodide ion drastically enhances posterior ionic diffusion or exchange in polymers. Such posterior diffusion means can be applied for functionalization for matrices with arbitrary shape or size, occasionally, beyond hydrophobicity. As an application for plating, "iodine doping" (and following "secondary doping") is available for metallic plating on hydrophobic matrices.

EXPERIMENTS: Samples are industrial products of micron-sized particles, which designed for ACF (anisotropic conduction film) or spacer with 2 or 5 mm diameters; they are synthesized as spherical particles of acryl resin showing fine-controlled dispersion of diameter. Some particles are products grafted with polystyrene (PS) on their spherical surface. [5]

These matrixes were "iodine-doped" by immersing in I_2-KI(aq) or I_2-NH_4I(aq) (0.1-3.0N) for more than one week. For "secondary doping" of Ag^+, each samples were immersed in $AgNO_3$(aq) (0.1-2.0M) for a few days.

On electroless Cu-plating in aqueous solution, THRU-CUP PSY (UYEMURA) was used. All operation were done at room temperature (c.a. 25℃).

RESULTS: As previously reported, since the resin beads samples have chemically hydrophobic surface as grafted PS, the non-treated sample powder can be little dispersed in water, and ionic treatment (ionic diffusion or electroless plating) for them can be also achieved hardly with ordinal aqueous solutions.[6] Nevertheless, process with the polyiodides aqueous solutions can easily introduce iodine on "(1st) iodine doping" and following Ag^+ ion on "secondary doping" into such hydrophobic surface; coloring with inner-diffused polyiodide (brown) or inner-precipitated AgI (light yellow) had been achieved in a few days or less.

Furthermore, electroless plating with aqueous "THRU-CUP PSY" can advance easily and actively; "iodine-doped" and following "Ag secondary-doped" micro beads, which was originated as hydrophobic surface, could be easily dispersed to aqueous solution of electroless plating reagent, bubbles of H_2 gas were created and light blue color of Cu ion vanished gradually. (Fig.1)

These results means that "iodine doping" (and following "secondary doping", occasionally) is available for posterior introduction of functionality into surface of polymeric materials. Such process has potential availability independent from shape or size of targeted objects, or from if polymeric region is ordered (crystallite) or non-ordered (amorphous), or from if the objects are hydrophilic or hydrophobic.

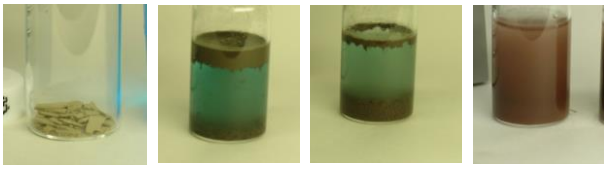

Fig.1: (a) micro particle after "iodine doping" and following "Ag-secondary doping" with $AgNO_3$(aq); (b)-(d) development after injection of electroless Cu-plating aqueous solution, "THRU-CUP PSY".

ACKNOWLEDGMENTS: These results are researched with Dr. Gotoh (Shinshu Univ.) and his staff and are partially funded by NEDO.[5]

REFERENCES:

[1] A. Kawaguchi, Polymer, **35**, 3797-3798. (1994)

[2] patent. JPN-5444559 (2014).

[3] KAWAGUCHI Akio, *et.al.,* SPring-8 User Exp. Rep. **5** (2000A), 354-354. (2000)

[4] A. Kawaguchi, Polym.Prep.Jpn., **62**,5116-5117. (2013).

[5] "Projects for Practical Use from Innovation" sponsored by NEDO (2007-2009).

[6] A. Kawaguchi, *et.al.,* KURRI Prog.Rep.2016, 78-78. (2017).

CO4-25 Compositional Dependence of Mössbauer Spectra for Fe_2O_3-Al_2O_3 Solid Solution

S. Takai[1], H. Nakaishi[1], H. Chen[1], T. Yabutsuka[1], T. Yao[2], S. Kitao[3], M. Seto[3]

[1]*Graduate School of Energy Science, Kyoto University*
[2]*Kyoto University*
[3]*Institute for Integrated Radiation and Nuclear Science, Kyoto University*

INTRODUCTION: While α-Fe_2O_3 and α-Al_2O_3 possess corundum-type structure, the reported solid solution ranges are restricted as approximately 10 % from the both end members due to the 5.6% smaller *c*-axis for Al_2O_3 compared with Fe_2O_3. In recent years, we have found that solid solution of $(Fe_2O_3)_{1-x}(Al_2O_3)_x$ is available for all the compositional range through the mechanochemical synthesis route. Although only the electrochemical property has been investigated on this solid solution system, further magnetic or physicochemical properties have not been clarified yet. Assuming that spin interaction of Fe is diluted by Al substitution, present Fe_2O_3-Al_2O_3 solid solution system is the model case to discuss the magnetization of the corundum-type structure, which has not achieved without the solid solution formation.

In the present investigation, as a relatively early study for the magnetism of Fe_2O_3-Al_2O_3 solid solution, we measured the Mössbauer spectra at room temperature for various compositions of $(Fe_2O_3)_{1-x}(Al_2O_3)_x$. Assuming that α-$Fe_2O_3$ shows weak ferromagnetism with canted magnetic structure at room temperature, contribution of the partial substation of aluminum is important. We focused on the variation of magnetism of the solid solution from the profile of Mössbauer spectra.

EXPERIMENTS: Stoichiometric mixture of γ-Fe_2O_3 and γ-Al_2O_3 reagents were put into a silicon nitride milling pod with 10 milling balls with the diameter of ϕ10. The compositions were selected as x = 0, 0.01, 0.25, 0.33, 050 and 0.67 for $(Fe_2O_3)_{1-x}(Al_2O_3)_x$ system. Mechanical alloying was carried out using a planetary ball milling machine operated at 800 rpm for 240 min. The crystalline phase of the obtained sample was confirmed by X-ray diffraction.

For the measurement of Mössbauer spectroscopy, ^{57}Co in Rh was employed as the γ-ray source. Doppler velocity scale has been calibrated by using Fe foil. The Mössbauer spectra were collected at room temperature. Lorentzian line shapes were assumed for the spectral profile analyses.

RESULTS: Fig. 1 shows the measured Mössbauer spectra for $(Fe_2O_3)_{1-x}(Al_2O_3)_x$. For the spectrum of the sample of x = 0 synthesized by milling γ-Fe_2O_3, sextet peaks were observed, which corresponds to the typical spectrum of α-Fe_2O_3. With increasing the amount of Al_2O_3, additional doublet peaks appear decreasing the sextet peaks. The profiles become almost doublet at x = 0.50 and only the sharp doublet can be seen for x = 0.67. This indicates that weak ferromagnetism diminishes with the substitution of aluminum ions to show the paramagnetic feature. From the sexted component, internal magnetic field is estimated from the peak position and plotted versus Al_2O_3 amount in Fig. 2. The deduced internal magnetic field decreases with x for $(Fe_2O_3)_{1-x}(Al_2O_3)_x$. Therefore, dilution with non-magnetic aluminum ions would reduce the long-range spin ordering to change the magnetic properties, and hence attribute to the internal magnetic field.

Additional experiments as magnetization, XAFS, or heat capacity measurements are now in progress. Precise magnetic behavior in this system would be investigated with these aspect as well as the present results.

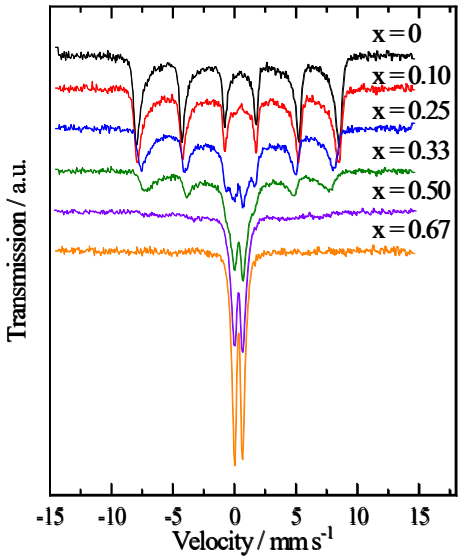

Fig. 1. Mössbauer spectra for $(Fe_2O_3)_{1-x}(Al_2O_3)_x$ measured at room temperature.

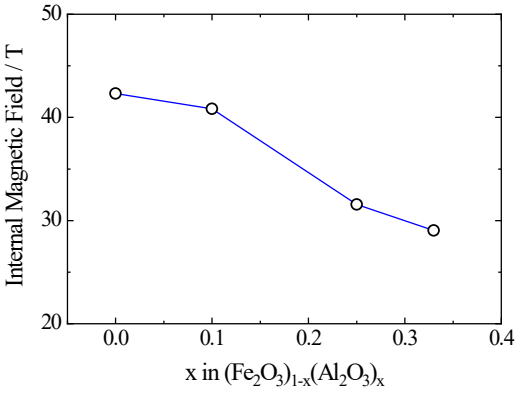

Fig. 2. Internal magnetic field of $(Fe_2O_3)_{1-x}(Al_2O_3)_x$.

REFERENCES:

[1] A. Muan *et al., J. Am. Ceram. Soc.*, 39 (1956) 207-214.
[2] S. Takai *et al., Solid State Ionics*, 313 (2017) 1-6.

CO4-26 Study of resonant frequency change with irradiation dose of piezoelectric PZT element

M. Kobayashi, T. Miyachi, S. Takechi[1], N. Konishi[1], Y. Morita

Planetary Exploration Research Center, Chiba Institute of Technology
[1]Graduate School of Engineering, Osaka City University

INTRODUCTION: In the previous studies, we have performed experiments that a piezoelectric element was irradiated with high intensity 400 MeV/n Xe beam at HIMAC of the National Institute of Radiological Sciences [1][2]. As a result, we found that when irradiating high intensity heavy ions to a piezoelectric element, its resonance frequency and anti-resonance frequency are shifted and also the impedance at the resonance frequency and anti-resonance frequency are changed by beam irradiation. Electromechanical coupling coefficient of the piezoelectric element is decreased.

Since the piezoelectric element is a crystalline material, it is considered that the crystal is damaged by the beam irradiation, and thus the characteristic parameter such as the resonance frequency has changed. Although it is considered to be some radiation damage, detailed mechanism such as its mechanism is not known.

Therefore, in this study, we investigated the response of the piezoelectric parameter to energetic electron beam which has dominantly ionizing effect (less non-ionizing effect).

EXPERIMENTS: From on from irradiation tests in the last year, we performed several runs in which piezoelectric elements were irradiated with electron beam in KURRI-LINAC as an electron beam source. For this year, we varied the condition of electron beam irradiating the test piece, current, energy and so on. There were three conditions in terms of input energy rate into the test PZT element, which were (A) 0.62kJ/sec, (B) 0.55kJ/sec and (C) 0.51kJ/sec. The test piece of PZT element have been warmed by the input electron beam energy, and in the same time, the pieces were air-cooled by a fan to prevent from warming up too much to maintain piezoelectricity. Hence, the temperatures of test pieces were at (A) 118ºC, (B) 100ºC and (C) 80ºC, respectively. Table 1 summarized the other experimental parameters as experimental conditions.

Table 1. Summary of experimental conditions

	Run (A)	Run (B)	Run (C)
Duration (min)	123	129	263
Beam energy (MeV)	18.8	15	20
Beam current (μA)	0.52	0.52	0.4
Input power (j/sec)	6.42	5.5	5.12
Achieved Temp (ºC)	118	103	80
Input energy rate (kJ/sec)	0.62	0.55	0.51

RESULTS: Qualitatively, the same results as last year's experiment were obtained. When irradiation is started, as the temperature of the PZT element rises, the resonance frequency of the PZT element also increases. The resonance frequency also increases with the irradiation amount after the temperature reaches equilibrium. The resonance frequency shift behavior during irradiation is different between Xe beam and electron beam, namely, during beam irradiation and warmed-up of the PZT test piece, the resonance frequency is shifted lower for Xe beam while the frequency is shifted higher for electron beam (in this study), in compared with one at room temperature.

Even after the irradiation is stopped, the resonance frequency is higher than that before the irradiation, while the electromechanical conversion coefficient was decreased, which is the same behavior as one in Xe beam experiment [1][2]. However, among the three tests summarized in Table 1, Run (C) does not have significant change in the electromechanical conversion coefficient. In fact, we performed three runs under the condition of (C) shown in Table1 and found no change in the electromechanical conversion coefficient.

Table 2 summarized the results of those runs and shows also the results of Xe beam experiment for comparison. Two things can be said from this result. First, although Run A and B have a change in the electromechanical conversion coefficient, Run C has no change. It is difficult to interpret this result. One assumption is that changes in the electromechanical conversion factor may require other conditions in addition to beam illumination. For example, the temperature must be above 100 ° C. We will verify this in future experiment.

The other is that the rate of change of the electromechanical conversion coefficient is about twice larger than that of the Xe beam irradiation experiment. Since it is thought that there is some uncertain factor in the estimation of the energy injection amount of the experimental result shown here, this will be further studied in the future.

Table 2. Summary of experimental conditions

	Electron beam (this study)			Xe beam
	Run (A)	Run (B)	Run (C)	
Decrease rate of electromechanical conversion factor[%/kJ]	0.126	0.124	0.0	0.22

REFERENCES:

[1] M. Kobayashi *et al.,* Japanese Journal of Applied Physics 53, 066602 (2014).
[2] M. Kobayashi *et al.,* Japanese Journal of Applied Physics 52, 126604 (2013).

CO4-27 Evaluation of Structural Vacancies in Icosahedral Cluster Solids using Positron Annihilation

J. Takahashi[2], R. Nakajima[3], K. Kitahara[1], A. Yabuuchi[3], N. Oshima[4], I. Kanazawa[2], A. Kinomura[3], K. Kimura[1]

[1]*Department of Advanced Materials Science, The University of Tokyo*
[2]*Department of Physics, Tokyo Gakugei University*
[3]*Institute for Integrated Radiation and Nuclear Science, Kyoto University*
[4]*National Institute of Advanced Industrial Science and Technology (AIST)*

INTRODUCTION: Since the discovery of icosahedral Quasicrystals(i-QCs), extensive studies of i-QCs have been devoted to clarify their structures and electronic transport properties. Unlike crystalline and amorphous metals, stable icosahedral Al-based quasicrystals exhibit anomalous "non-metallic" properties. The term "non-metallic" means a high electrical resistivity and its large negative temperature coefficient. Kimura et al [1] have indicated that the vacant centers of the icosahedral clusters play an important role for stabilities and chemical bonding nature of cluster. Kirihara et al. [2] have reported that 12-Al icosahedral cluster, of which the center of the first shell of cluster is vacant, have covalent bonding nature, while 13-atoms icosahedral cluster with a central atom have metallic bond nature. Positron annihilation method is powerful one for detecting structural vacancies of quasicrystals [3]. Recently Kimura and coworkers [4] have estimated structural vacancies for 1/1-AlReSi approximant crystals by positron annihilation spectroscopy. Positron annihilation measurement of the positron lifetime, coincidence Doppler broadening (CDB), and depth profiling by slow positon beams have shown that structural vacancies in the order of 10^{-3} , which are identified to be centers of the first shell of icosahedral clusters. They found that the structural vacancy density of metallic 1/1 AlReSi with less Re is lower than that of no-metallic AlReSi with more Re. In this study, we have measured the Doppler broadening of quasicrystal AlPdRu, 2/1 approximant crystal AlPdRu, and 1/0 approximant crystal AlPdRu.

EXPERIMENTS and RESULTS:
By using the slow positron beam, we have estimated the change in S-parameter with positron-incident energies in quasicrystal AlPdRu, 2/1 AC AlPdRu, and 1/0 AC AlPdRu. Figure 1 shows the change in S-parameter with positon-incident energies in quasicrystal AlPdRu. The closed circles show the S-parameter, and the open squares show the total counts within the positron annihilation spectra. As shown in Figure 1, S-parameter seems to increase as the positron-incident energy increases from ~0 to 2 keV. But the fluctuation of the values of S-parameter is relatively large. The important point is that the total counts of the positon annihilation spectra decrease remarkably below the positron-incident energy ~ 2keV. So, in order to obtain better data, we must measure the annihilation spectra for longer accumulation time below the positron-incident energy ~ 2 keV.

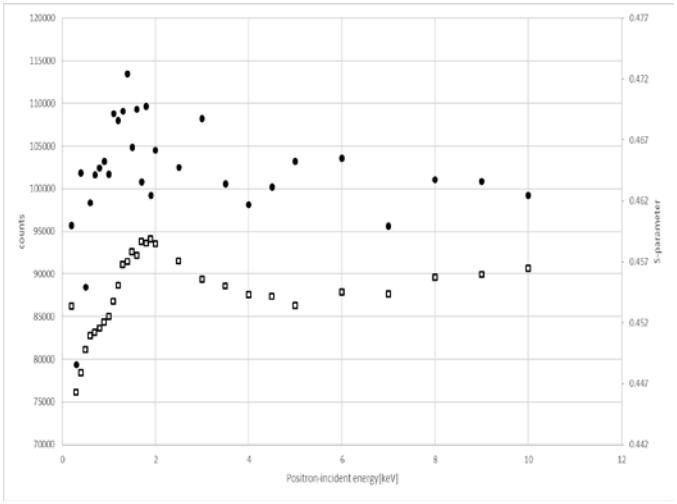

Fig. 1. The closed circles show the S-parameter of quasicrystal AlPdRu. Open squares show the total counts of the positron annihilation spectrum.

REFERENCES:
[1] K. Kimura *et al.*, J. Solid State Chem. **133** (1997) 302.
[2] K. Kirihara *et al.,* Phys. Rev. Lett. **85** (2000) 3468.
[3] I. Kanazawa *et al.,* Phys. Rev. Lett. **79** (1997) 2269.
[4] K. Yamada *et al.,* Philog. Mag. **98** (2018) 107.

CO4-28 Porosity Measurements of Sintered-Silver Bonding Plates

K. Wakamoto[1], T. Otsuka[1], K. Nakahara[1], A. Yabuuchi[2] and A. Kinomura[2]
[1]*Power Device R&D Department, ROHM Co., Ltd.*
[2]*Institute for Integrated Radiation and Nuclear Science, Kyoto University*

INTRODUCTION: Sintered silver has attracted much attention as a die-attach material for the power electronics, owing to its high heat dissipation capability [1]. On the other hand, the coefficient of thermal expansion (CTE) inevitably does not match each other of the materials used in a power system. Thus the heat-cycle oriented mechanical stresses deteriorate die-attach materials, and therefore the mechanical properties of sintered silver impinge on the reliability of electricity systems.

However, nobody can predict how long sintered silver sustains, because the material is porous and its mechanical properties heavily depends how porous it is. Accordingly, the research is highly demanded to measure the porosity.

The porosity rate (p) of sintered silver is reported by some papers [2-3], where p is measured by using cross sectional scanning electron microscopy (SEM). These studies focus on only the μm-order pores of sintered silver materials, not nm-order pores such as crystalline defects. Positron lifetime measurement method has advantages for this purpose. To this end, therefore, the authors used a conventional positron annihilation lifetime spectrometer in Kyoto University to estimate the nm-order pore sizes embedded in sintered silver with various p's by measuring the positron lifetime of the material.

EXPERIMENTS: Four samples were prepared for this research. The fabrication process is described as follows.

Paste including silver nm-particles was stencil printed on a metal plate, and the containing organic solvent was dried at 140ºC for 1 h. These dried films were sintered at 300 ºC for 10 min with uniaxial press via a carbon buffer sheet with 5-, 10-, and 60-MPa pressure. The film shape were 5 mm square and 40-μm thick. As reference, a 500-μm bulk silver sheet annealed at 550 ºC for 2 h was prepared. The process pressure used and the p of each sample are shown in Table I.

Table I Material, pressure, and p of the specimens.

Sample		Material	Pressure (MPa)	p (%)
A		Bulk silver	–	–
B		Sintered silver	60	5
C		Sintered silver	10	14
D		Sintered silver	5	25

p is determined by using cross-sectional SEM images. p is 5%, 14%, and 25% for sample B, C, and D, respectively.

Positron annihilation lifetime spectroscopy was performed to evaluate bulk lifetimes of the samples by using a ^{22}Na source sealed with 7.5 μm Kapton foils. The thickness of the samples B, C, and D was approximately 40 μm. Five sample plates were stacked and measured together to stop all the positrons from the source inside the samples. The spectrometer consists of two scintillation gamma-ray detectors with BF_2 crystals and a digital oscilloscope.

RESULTS: Fig. 1 shows the positron lifetime spectra for the samples B and D together with the reference Ag. The lifetime spectra were decomposed into one or two components apart from the source component. A lifetime of 0.138 ns was obtained for the reference Ag and it was in good agreement with the Ag lifetime previously reported. Average lifetime of the samples B, C and D decreased from 0.24 to 0.22 with increasing pressure during sample formation. Two component analysis of the lifetime spectra showed that the first lifetime changed in the range of 0.17 – 0.20 ns, while the second lifetime changed in the range of 0.29 – 0.33 ns. Changes of lifetimes as a function the formation pressure were not simple, differently from those of the average lifetimes. Balance between the first and second lifetimes changed with increasing the pressure. Further analyses are required to clarify the origin of each lifetime component.

In summary, porosity of sintered Ag plates was characterized by conventional positron annihilation lifetime spectroscopy. The preliminary data were successfully obtained suggesting the correlation between the positron lifetime and the formation pressure.

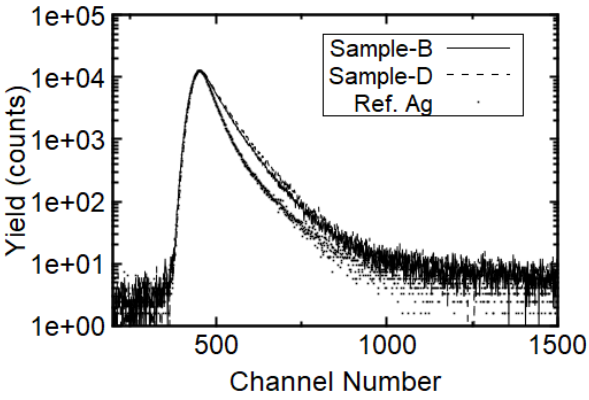

Fig. 1 Typical lifetime spectra of the samples.

REFERENCES:

[1] KIM S. SIOW, Journal of ELECTRONIC MATERIALS., **43** (2014) 947-961.
[2] T. Yousseff *et al*., Microelectronics Reliability., **55** (2015) 1997-2002.
[3] M. Takesue *et al*., Proc. PCIM., (2018) 14

CO4-29 Radiation Resistivity of Ferrite Permanent Magnets Against Neutrons

Y. Iwashita[1], M. Abe[1], T. Yako[1], T. Kurihara[2], M. Fukuda[2], M. Sato[2], T. Sugimura[2], Y. Iinuma[3], Y. Fuwa[3] and K. Takamiya[3]
[1]*Institute for Chemical Research, Kyoto University*
[2]*Accelerator Laboratory, KEK*
[3]*Institute for Integrated Radiation and Nuclear Science, Kyoto University*

INTRODUCTION: Permanent magnets are used as material of beam optical elements. While rare earth magnets, such as neodymium and samarium cobalt, are known to have radiation demagnetization [1], there is not enough information for ferrite magnets, which are economical but have less remanent field strength. In order to verify the resistivity of ferrite magnets, we carried out a trial experiment on radiation demagnetization of ferrite magnets irradiated by neutrons at Kyoto University Research Reactor (KUR).

EXPERIMENTS: We purchased cylindrical anisotropic ferrite magnets with 10 mm diameter and 10 mm length that have easy-axis parallel to the cylinder axis. Since they seemed to have common non-uniformity on the easy-axis and they were randomly magnetized, they were re-magnetized to have better magnetic uniformity. We measured their magnetic field at both end surfaces with a Tesla meter (SENIS 3MH3) using a magnet fixture jig prepared for this experiment. The jig has a 0.5 mm thick plastic plate between the Hall probe and the magnet end surface to avoid a direct contact between them. The irradiation times were starting from 10 seconds and up to maximum 4 hours at 1 MW operation, and 12 minutes and 36 minutes at 5 MW operation. A permanent magnet sample packed in a polyethylene bag was placed into a capsule together with absorbent cotton and sent to the reactor by pneumatic transporter. After the residual radioactivity of the magnet and capsule decayed sufficiently, we took out the magnet sample from the capsule and measured the magnetic field. We compared the magnetic field strength before and after irradiation.

RESULTS: Fig. 1 shows the ratios of the magnetic field strength before and after the irradiation. The error bars show the standard deviations of measured data for each magnet. The resulted data points scatter wider than the error bars, which may come from the magnet fixture configuration of the jig and the measurement procedure. Since the magnets were measured with the polyethylene bag, the distance between the Hall probe and the magnet may not have been defined well, which can be improved for next experiment. In spite of the scattered data points of this preliminary experiment, we conclude that radiation demagnetization of ferrite magnets was not significant up to the range of irradiated dose. The blue line in Fig. 1 denotes neutron dose at which radiation demagnetization becomes significant for neodymium magnets[1]. Ferrite magnets were found to be more resistant to the radiation than neodymium magnets. According to the data taken so far, neutron dose of about 2×10^{18} seems necessary even for 10% reduction of magnetization. Fig. 2 shows comparisons of ratios of magnetic field on 1MW and 5MW operation, showing more decrease at 5MW. Since the temperature in the reactor at 5MW operation is higher than at 1MW, the magnet temperature may have affected the demagnetization process. More data points are desired for better understanding, and the threshold level may become clear.

PERSPECTIVES: More irradiation dose with improved magnetic field measurement procedure will clarify the demagnetization as a function of the dose level.

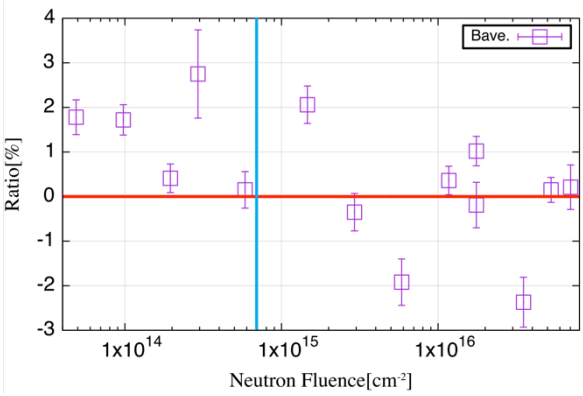

Fig. 1: Ratio of radiation demagnetization of ferrite permanent magnet.

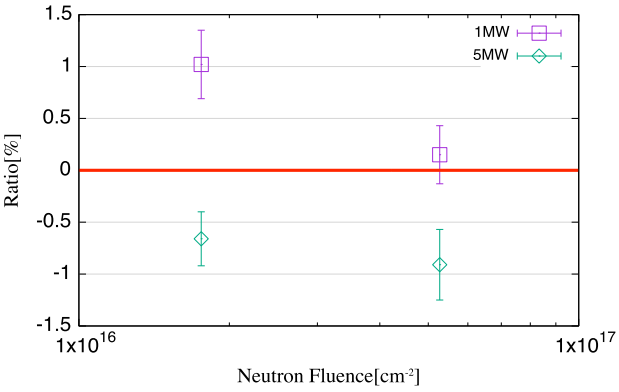

Fig. 2: Ratio of radiation demagnetization on 1MW and 5MW operation.

REFERENCES:

[1] X. -M. Marechal, T. Bizen, Y. Asano, H. Kitamura, Proceedings of EPAC, Edinburgh, Scotland, 2006.

CO4-30 Neutron Irradiation to Optiacal Devices for ITER Diagnostics System

E. Yatsuka and M. Ishikawa,

Fusion Energy Research and Development Directorate, National Institutes for Quantum and Radiological Science and Technology (QST)

INTRODUCTION: QST is developing Diagnostic systems for ITER, which is a fusion experimental reactor. In the development, it is important to verify the radiation resistance of each component of the Diagnostic systems, in particular, the neutron resistance. The purpose of this study is that the high neutron flux generated from Kyoto University Research Reactor (KUR), which is equivalent to the fluence experienced by the diagnostic components during 20 years operation of ITER, irradiates to the component. Then, it is clarified whether the performance of the optical element can be maintained even after high neutron irradiation.

EXPERIMENTS: Neutron irradiation to the optical element (main material is SiO_2) for ITER Edge Thomson Scattering System [1], which is one of the diagnostic system procured by Japan Domestic Agency is performed at the Slant Exposure Tube in KUR in order to investigate the degree of deterioration of the element.

RESULTS: After 20 hours of neutron irradiation at the Slant Exposure Tube, the surface dose rate of the irradiated optical device was measured. It was found that it was relatively high (>300μSv/h: immediately after irradiation, $\gamma \sim 50$ μSv/h, $> \beta\ \gamma 300\mu$ Sv/h). Therefore, it was decided that optical measurements of the irradiated optical element would be performed the next fiscal year (FY2019)

REFERENCES:

[1] E. Yatsuka, T. Hatae, M. Bassan, *et. al.,* Fusion Eng. Design, **100** (2015), 461-467.

CO4-31 A study on destruction of cesium aluminosilicate compounds by gamma ray irradiation

H. Ohashi, R. Takaku, T. Saito[1]

Faculty of Symbiotic Systems Science, Fukushima University
[1]Institute for Integrated Radiation and Nuclear Science, Kyoto University

INTRODUCTION: In recent years, aluminosilicate compounds have attracted attention as a final disposal method of ^{137}Cs contained in radioactive contaminated waste. One of the most considered to be a promising material is pollucite. Pollucite has various properties that favor the immobilization of Cs ions, and in situ synthesis from soil is also possible [1]. However, the damage to the aluminosilicate framework by radiation decay is concerned because it contains ^{137}Cs. Several reports have been made on the effect by β-decay of ^{137}Cs on aluminosilicate framework [2, 3], and no significant damage to the framework has been confirmed in any of the reports. On the other hand, the effects of gamma rays have not been reported. The purpose of this study was to investigate the influence of gamma rays on the synthesized pollucite with aluminosilicate framework.

EXPERIMENTS: The solution with Na_2SiO_3, $NaAlO_2$, CsCl, NaOH, and water was prepared and placed in a Teflon inner cylinder pressure container. Pollucite was synthesized by hydrothermal method, holding the container at 180 ℃ for 5 hours. The resulting precipitate was washed and collected by filtration, and dried at 110℃ for 16 hours at least.

The powder samples were irradiated with ^{60}Co gamma rays at 228 kGy. Characterization was performed by XRD. The 7 days leaching test by PCT-A method was carried out to evaluate the change of Cs retention performance by framework damage. The normalized leaching rate, NR_i [g/m^2·d], was calculated by equation (1).

$$\mathrm{N}R_i = \frac{c_i}{f_i \frac{SA}{V} t} \qquad (1)$$

Where c_i [g/L] was the concentration of element "i" in the solution, f_i was the weight ratio of the element "i" in the sample before leaching, SA [m^2] was the sample surface area, V [L] was the volume of the leaching liquid, and t [day] was the test duration.

RESULTS: Fig.1 shows the XRD patterns of pollucite sample and gamma irradiated pollucite. All the patterns showed that they contained only single-phase pollucite, and gamma irradiated pollucite did not significantly change compared to pollucite without irradiation, indicating that there was no change with irradiation in the crystal structure in bulk phase.

Table 1 shows the various parameters obtained by the leaching test according to the PCT-A method, and the normalized leaching rate. In previous report [4], the normalized leaching rate of pollucite was around 10^{-5} to 10^{-6} g/(m^2·d), and was close value to the sample with gamma ray irradiation at this study.

From the above results, it was considered that the effect of gamma ray irradiation on the aluminosilicate framework of pollucite was not observed in this study.

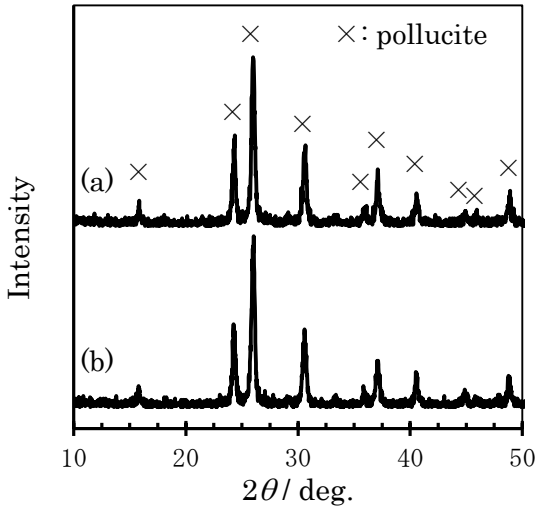

Fig. 1. XRD patterns of (a) pollucite and (b) γ-irradiated-pollucite

Table 1. Leaching test parameters in this study

	f_{Cs}	SA/V [m^2/L]	NR_{Cs} [g/m^2·d]
pollucite	0.40	3.1×10^{3}	1.1×10^{-6}
γ-irr.-pollucite	0.40	3.1×10^{3}	1.0×10^{-6}

REFERENCES:

[1] Y. Yokomori *et al.*, *Sci. Rep.*, **4** (2014), 4195
[2] J. Fortner *et al.*, Radiogenic transmutation effects in a crystalline aluminosilicate ceramic: a TEM study, Scientific Basis for Nuclear Waste Management XXV Materials Research Society 2001 Fall Meeting, November 26–30 2001, Boston, Massachusetts.
[3] N. J. Hess *et al.*, *J. Nucl. Mater.*, **281** (2000), 22-33.
[4] Z. Jing *et al.*, *J. Hazard. Mater.*, **306** (2016), 220–229.